Journal Pre-proofs

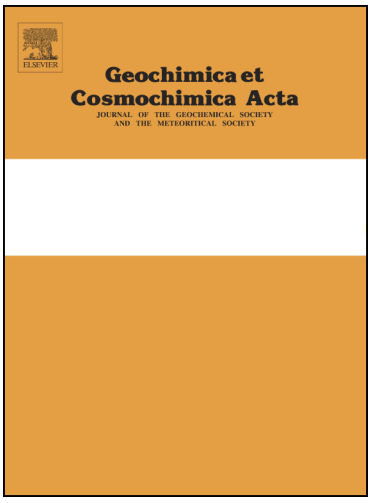

Boron isotope fractionation during adsorption on aragonite and calcite in artificial seawater and NaCl aqueous solutions

Giuseppe D. Saldi, Pascale Louvat, Frank Heberling, Vasileios Mavromatis, Jacques Schott

PII: S0016-7037(25)00639-8
DOI: https://doi.org/10.1016/j.gca.2025.11.032
Reference: GCA 14106

To appear in: *Geochimica et Cosmochimica Acta*

Received Date: 17 June 2025
Accepted Date: 18 November 2025

Please cite this article as: Saldi, G.D., Louvat, P., Heberling, F., Mavromatis, V., Schott, J., Boron isotope fractionation during adsorption on aragonite and calcite in artificial seawater and NaCl aqueous solutions, *Geochimica et Cosmochimica Acta* (2025), doi: https://doi.org/10.1016/j.gca.2025.11.032

Boron isotope fractionation during adsorption on aragonite and calcite in artificial seawater and NaCl aqueous solutions

Giuseppe D. Saldi[a,b,*], Pascale Louvat[c], Frank Heberling[d], Vasileios Mavromatis[e], Jacques Schott[a]

[a] *Géosciences Environnement Toulouse (GET), Observatoire Midi-Pyrénées, Université de Toulouse, CNRS, IRD, UPS, 14 Avenue Edouard Belin, 31400 Toulouse, France*

[b] *Dipartimento di Fisica e Geologia, Università di Perugia, via Pascoli snc, 06123 Perugia, Italy*

[c] *Université de Pau et des Pays de l'Adour, IPREM, CNRS-UMR 5254, 640000 Pau, France.*

[d] *Karlsruhe Institute of Technology (KIT), Institute for Nuclear Waste Disposal (INE), Hermann-von-Helmholtz-Platz 1, D-76344 Eggenstein-Leopoldshafen, Germany*

[e] *Institute of Geological Sciences, University of Bern, Baltzerstrasse 1+3, 3012 Bern, Switzerland*

* Corresponding author

E-mail address: giuseppe.saldi@unipg.it

Keywords: Boron isotope fractionation; adsorption; Three-plane model; seawater; calcite; aragonite.

ABSTRACT

Adsorption of dissolved species on mineral surfaces is a key elementary process, which controls crystal growth and incorporation of trace elements into mineral structures, affecting the isotopic composition of geological archives. Changes of chemical composition of aqueous solution can induce significant variations in the type, concentration and isotopic composition of boron surface species incorporated by $CaCO_3$. To better understand and quantify these effects, the boron isotope fractionation associated with B adsorption on calcite and aragonite was investigated in artificial seawater and equimolar solutions of NaCl (0.5 M) at room temperature and $7.5 \leq pH_{NBS} \leq 11.9$. Boron adsorption on aragonite was 2-4 times stronger than on calcite, in agreement with the higher affinity of aragonite for borate ions reported by previous studies. In seawater solutions at pH > 8.5, B removal from the solution increased due to increasing adsorption on both $CaCO_3$ polymorphs and coprecipitation with brucite, which was observed to form at more alkaline conditions. Boron sorption reactions on calcite and aragonite surfaces were described using the calcite three-plane model (TPM) assuming the presence of a borate inner-sphere complex ($> BO_3H_2^{+0.5}$), formed by the replacement of $B(OH)_4^-$ for surface carbonate groups, and the adsorption of $B(OH)_4^-$ at calcium protonated sites ($>[CaOH_2^{+0.5}\cdots B(OH)_4^{-1}]^{-0.5}$). The relative distribution of the two species and the associated isotope fractionation factors were different for calcite and aragonite and changed between artificial seawater and NaCl solutions. On calcite the two surface complexes were heavier than aqueous borate, showing an overall fractionation of +5.5 to +6.4 ‰ in NaCl solutions ($7.8 \leq pH_{NBS} \leq 10.3$), the inner-sphere complex being ~3‰ heavier than the outer-sphere complex and 7.7 ‰ heavier than $B(OH)_4^-$. The isotope fractionation decreased to +4.7 ‰ in seawater ($7.9 \leq pH_{NBS} \leq 8.9$), where the inner-sphere complex accounted for > 99% of adsorbed boron. On aragonite the inner-sphere complex formed in NaCl 0.5 M resulted heavier than aqueous borate by 4.2 ‰, whereas the outer-sphere complex, accounting for 9 to 52 % of adsorbed boron between pH 8 and 11, exhibited the same isotopic composition as the aqueous anion. The overall isotopic fractionation varied from +4.1 ‰ (pH_{NBS} = 8.2) to +1.2 ‰ (pH_{NBS} =11.3). In seawater both borate surface species formed on aragonite were heavier than in NaCl solutions, resulting in overall fractionations of about +4.05 ±0.05 ‰ relative to aqueous $B(OH)_4^-$.

The present analysis of boron adsorption and isotope fractionation suggests that the isotopic composition of borate ions adsorbed on $CaCO_3$ in seawater is affected by the specific interaction of the carbonate surface with different aqueous ions, such as SO_4^{2-}, which modifies the local surface structure favoring the adsorption of $B(OH)_4^-$ ions that are either lighter (calcite) or heavier (aragonite) relative to NaCl solutions. These findings illustrate the complex behavior of boron upon adsorption on $CaCO_3$ and support the need for studies that provide a more comprehensive description of the processes by which boron isotopes are incorporated and fractionated during biogenic and abiogenic $CaCO_3$ formation in seawater.

1. INTRODUCTION

The boron content and isotopic composition of marine carbonates, such as planktonic foraminifera and corals, have been successfully used for over thirty years to reconstruct past ocean pH and corresponding CO_2 atmospheric levels (Foster and Rae, 2016; Henehan et al., 2020; Rae et al., 2021; CenCO2PIP Consortium et al., 2023). They also provide insights into the biomineralization processes by which boron is incorporated in the shells and skeletons of these living organisms (e.g., McCulloch et al., 2012; DeCarlo et al., 2018). The success and accuracy of the boron isotope pH-proxy strongly depend on empirical calibrations based on culture experiments of different marine species of corals and foraminifera (Trotter et al., 2011;

Henehan et al, 2013; Foster and Rae, 2016; Coenen et al., 2024). The $\delta^{11}B$ of biogenic $CaCO_3$ is generally a well-defined function of seawater pH but exhibits for most species a systematic offset relative to the corresponding $\delta^{11}B$ of the borate ion that should control their isotopic composition (Foster and Rae, 2016; Hönisch et al., 2019). The observed differences in $\delta^{11}B$ values between marine carbonates and the free borate ion have been explained with physiological processes regulating the internal pH of the calcifier or with changes in the microenvironmental conditions in vicinity of the growing carbonate structure (Hönisch et al., 2003; Rollion-Bard and Erez, 2010; Anagnostou et al., 2012; Venn et al., 2013). Although the role of the various physiological parameters is poorly constrained, the $\delta^{11}B$ record of marine biogenic carbonates has been generally considered consistent with the fundamental assumptions of the paleo-pH proxy established by Hemming and Hanson (1992): only borate ion is incorporated in the mineral structure; no B isotopic fractionation occurs during uptake by $CaCO_3$.

Nevertheless, recent experimental and theoretical studies have questioned the general validity of such hypotheses. Inorganically-precipitated calcites were reported to have a heavier B isotopic composition relative to the corresponding composition of aqueous $B(OH)_4^-$ (Sanyal et al., 2000; Noireaux et al., 2015; Farmer et al., 2019; Henehan et al., 2022), whereas boron co-precipitated with aragonite did not exhibit any evident fractionation, in agreement with the basic assumptions of the pH-proxy tool (Noireaux et al., 2015; Henehan et al., 2022). Mavromatis et al. (2015) and Noireaux et al. (2015) reported NMR data showing the presence of trigonal boron in inorganically precipitated calcite. This evidence, together with the heavier B isotopic composition of inorganic calcite and its weaker dependence on pH, could be related to the incorporation of small amounts of $B(OH)_3$, likely controlled by surface kinetic effects (Uchikawa et al., 2015; Kaczmarek et al., 2016; Branson, 2018; Farmer et al., 2019). Henehan et al. (2022) suggested that the observed isotope fractionations might also result from kinetic effects induced by the electrostatic interaction of ion pairs, namely $CaB(OH)_4^+$, attracted to the mineral surface by a negative electrostatic potential gradient. According to the surface kinetic model of B incorporation proposed by Branson (2018) and Farmer et al. (2019) the B content and isotopic composition of grown calcites is a function of the relative attachment and detachment partitioning of $B(OH)_3$ and $B(OH)_4^-$. Slower precipitation rates should favor the weak stochastic attachment of $B(OH)_3$, resulting in higher $\delta^{11}B$ of the mineral compared to the corresponding $\delta^{11}B$ of aqueous $B(OH)_4^-$. This conclusion is in apparent contrast with the boron adsorption behavior described by Saldi et al. (2018), who showed that only $B(OH)_4^-$ can be adsorbed by the calcite surface at equilibrium conditions, forming surface complexes that are 2 to 5 ‰ heavier than aqueous borate. This implies that during adsorption-controlled growth at close-to-equilibrium conditions the observed boron isotope fractionation of calcite should be the result of the incorporation of heavier borate ions and not derive from the attachment of small amounts of $B(OH)_3$. It should be also noted that the formation of calcite and aragonite via an amorphous calcium carbonate precursor (ACC) (Mavromatis et al., 2021) promoted the incorporation of both trigonal and tetragonal B incorporation in the resulting crystallized calcite and aragonite with significant enrichments in heavy B isotopes compared to aqueous borate. This finding, which contradicts the paleo-pH proxy assumption, agrees with the results of quantum-mechanical calculations (Balan et al., 2018; Yin et al, 2023) that predict a significant equilibrium isotope fractionation between borate incorporated in calcite or aragonite and aqueous borate (+9.8‰ and + 7.2‰ for calcite and aragonite, respectively). From this agreement Mavromatis et al. (2021) concluded that the mechanisms operating during carbonate mineral formation from an ACC precursor are likely leading to near isotope equilibrium conditions between B in the solid and B aqueous species.

It is noteworthy that the above-cited experimental studies reporting a significant B isotope fractionation during co-precipitation and adsorption on calcite were conducted using NaCl aqueous solutions of different ionic strength containing Ca and Mg ions but in the absence of other relevant species dissolved in seawater (SO_4^{2-}, Sr^{2+}, K^+) (cf. Henehan et al., 2022; Uchikawa et al., 2023). Changes in ionic strength and aqueous solution compositions can significantly affect the rates of incorporation and chemical environment of boron in $CaCO_3$. For instance, it was observed that substitution of Na^+ for Ca^{2+} in the calcite structure promotes the boron incorporation by maintaining the local charge balance but might also affect the isotopic composition of boron co-precipitated or adsorbed on calcite (Uchikawa et al., 2017; Henehan et al., 2022; Uchikawa et al., 2023). The slightly lighter composition of adsorbed borate in solutions of NaCl 0.1 M relative to solutions of NaCl 0.01 M (Saldi et al., 2018) is also consistent with such an indication. The effects of oxyanions (SO_4^{2-} and HPO_4^{2-}) on the boron behavior during calcite growth were recently investigated by Uchikawa et al. (2023). The authors showed that the addition of 5 mmol of SO_4^{2-} to the growth solution brought about the decline of the growth rates by a factor of 3, leading to a significant increase (~ 3×) of the B/Ca ratio in calcite. The increase in boron content was accompanied by a 2.8‰ decrease in its isotopic composition relative to the control experiment without SO_4^{2-}. Such a change in calcite $\delta^{11}B$ and B/Ca was explained by the lattice distortion induced by the incorporation of SO_4^{2-}, which favored the uptake of the relatively smaller $B(OH)_4^-$ in the mineral structure with a reduced isotope fractionation compared to sulfate-free solutions. In the same study, Uchikawa et al. (2023) reported a similar effect on boron behavior by dissolved phosphate species.

The evidence brought by the earlier works underlines the need for a further understanding of the inorganic processes that control B incorporation by calcite and aragonite in seawater and the resulting isotopic composition of this element. The fundamental mechanisms governing boron co-precipitation with $CaCO_3$ in seawater have not been characterized in their complexity and deserve some systematic studies. In this contribution we studied the adsorption of boron on calcite and aragonite in artificial seawater and an equimolar solution of NaCl, as this process is expected to control the B incorporation and isotope composition during growth from weakly supersaturated solutions. Adsorption data were interpreted using the most recent surface complexation model of the calcite/water interface to characterize the boron complexes forming on the surface of the two $CaCO_3$ polymorphs and determine their isotopic composition. The presented results improve our understanding of boron interaction with the calcite and aragonite surfaces and should allow for a better estimate of the B isotope composition acquired during inorganic versus biotic $CaCO_3$ precipitation in marine environments.

2. MATERIALS AND METHODS

2.1 Calcite and aragonite powders

Boron adsorption on calcite and aragonite was studied on synthetic $CaCO_3$ minerals with high specific surface area. The calcite powder was acquired from Solvay and consisted of sub-micrometric particles with a platy and slightly rounded shape and dimensions ranging from 30 to 180 nm, with an average size of ~75 nm, as observed by transmission electron microscopy (TEM, JEOL JEM ARM-200F). X-ray powder diffraction (XRPD) analyses, conducted with a Bruker D8 diffractometer equipped with a Cu anode ($CuK\alpha_1$ = 1.54060 Å), and TEM analyses allowed verifying the bulk crystallinity of this solid sample. Two TEM images of these calcite particles are provided in Fig. 1.

Aragonite was synthesized in the laboratory from reagent grade Na_2CO_3, $CaCl_2 \cdot 2H_2O$ and $SrCl_2 \cdot 6H_2O$ according to a modified version of the synthesis protocol followed by Tadier

et al. (2017). Briefly, two solutions 0.1 M of Na_2CO_3 and $CaCl_2$ containing 1 mM $SrCl_2$ were rapidly mixed at 95 °C; the three-component aqueous solution was agitated for ~ 10 seconds, during which the incipient nucleation of aragonite crystals occurred. The obtained suspension was then immediately vacuum-filtered through a 0.20 μm polyamide membrane. The collected precipitate was rinsed successively with double-deionized (DDI) water and ethanol, placed on a watch glass and dried in an oven at 95°C. This procedure was repeated several times in order to obtain an amount of aragonite powder sufficient to conduct the entire series of experiments planned for the study. The synthetic aragonite powder consisted of aggregates of elongated acicular crystals 5-20 μm in length and less than 1 μm in cross-section (Fig. 2). As evidenced by the SEM analysis, aragonite needles appear to be formed by the agglomeration of smaller crystalline microplates, providing the acicular crystal with a complex surface micro-morphology. XRD analyses showed that the produced powder was mostly composed of aragonite with a negligible amount of calcite (< 2%).

The specific surface area (SSA) of calcite and aragonite powders was determined by 11-point adsorption isotherm according to the BET method using N_2 as adsorbate. The resulting SSA_{BET} values were equal to 22.67 and 4.31 m^2/g for calcite and aragonite, respectively. The uncertainties of both measurements are estimated to be ± 5%.

2.2 Boron adsorption experiments

B adsorption experiments were carried out in 50 ml polypropylene (PP) centrifuge tubes at room temperature (~ 25 °C) in artificial seawater (ASW), Mg-depleted ASW and NaCl solutions of the same ionic strength (NaCl 0.5 M) prepared from DDI water and analytical grade NaCl, $CaCl_2 \cdot 2H_2O$, $MgCl_2 \cdot 6H_2O$, KCl, Na_2SO_4 and $SrCl_2 \cdot 6H_2O$. The synthetic seawater preparation was based on the recipe adopted by Zhang et al. (2021), but without the addition of $NaHCO_3$. The composition of the low-Mg ASW was prepared according to the same protocol but using ~55 times less Mg-chloride than for the standard seawater. The composition of the two seawater solutions prepared for this study is reported in Table 1. The alkalinity of the initial seawater solutions was effectively nil and controlled by the amount of $CaCO_3$ dissolved during each experiment. Between 6 and 8 g of mineral powder and 25 g of electrolyte solution were used for each experiment, which corresponds to a solid-to-liquid ratio of 279-320 g/L. Boron stock solutions at 125 ppm were prepared by dissolving analytical grade boric acid into the same ASW and NaCl aqueous solution prepared for the experiments. Previous work conducted by Saldi et al. (2018) showed that no B was released nor adsorbed by the walls of the PP tubes used in this study after rinsing in acid and during interaction with B-bearing solutions at different pH values. So, no other tests were made to assess the potential release or loss of boron between the aqueous solutions and the container surfaces.

For each adsorption experiment the aqueous solution was equilibrated with the calcite/aragonite powder within the centrifuge tubes for ~ 3 days by continuous mixing of the suspension on a tube rotator. The pH of each suspension was adjusted to the desired value by addition of small amounts of HCl or NaOH 1 M. At the end of the equilibration period 1 ml of B stock-solution was added to each test tube to obtain a starting B concentration of ~ 5 ppm, to replicate the current seawater B concentrations (cf. Foster et al., 2010). The adsorption reaction in NaCl solutions was observed to be fast, reaching equilibrium within few hours (Saldi et al., 2018). We observed a similar boron behavior for aragonite and calcite reacting in ASW, with constant adsorbed concentrations attained after 24 hours. Following these kinetic tests, the suspensions of calcite and aragonite were exposed to aqueous B solutions for 48-52 h. Once agitation was stopped the suspensions were centrifuged for 25 min at a speed of 8000 rpm. A small volume of the solution separated from the solid (1.5-2 ml) was poured into a small

cylindrical tube for the pH measurement, whereas the remaining solution was withdrawn and filtered with a sterile plastic syringe through a hydrophilic 0.20 μm PTFE Millipore filter, acidified with ultrapure concentrated (14.5 M) HNO_3, and stored in a fridge before chemical analyses. pH measurements were conducted using a Metrohm glass microelectrode previously calibrated using NIST certified buffers (pH 4.01, 7.00, 10.01). As such pH measurements in this study are expressed according to the NBS-scale and denoted by "pH-NBS" hereafter (cf. Millero et al., 1993).

2.3 Boron adsorption-coprecipitation with secondary phases

The study of boron sorption behavior in seawater involves the interaction with other dissolved species and the interference with secondary phases that might form when the solution pH is adjusted to increasingly basic values. To assess the possible precipitation of secondary phases, such as brucite, from alkaline ASW solutions and their effects on the measured boron partitioning between the aqueous solution and the solid phases two different series of experiments were carried out in the absence of calcite and aragonite. These experiments were conducted for increasing amounts of NaOH 1M (0.2, 0.3, 0.6, 1.1 μL) added to the artificial seawater solutions. The same volumes of NaOH 1M were used during the adsorption experiments on calcite and aragonite in ASW. In the first series of experiments (BM) boron was added after the addition of the base, whereas in the other series of four experiments (BQ), the aqueous solutions were basified using the same volumes of NaOH 1M after that boron was added to the starting solutions. This approach allowed estimate of the amounts of boron potentially adsorbing and co-precipitating with secondary phases forming at more basic pH conditions.

2.4 Fluid chemical analyses and thermodynamic calculations

The aqueous concentrations of B, Ca, Mg, K, Sr and S were measured by inductively coupled plasma optical emission spectroscopy (ICP-OES) using a Horiba Ultima 2 spectrometer equipped with a nebulizer and a cyclonic spray chamber made of Teflon and Peek to prevent boron contamination and memory effects due to the sample contact with glass parts and thus improve the accuracy of the measurements (cf. Sah and Brown, 1997). All measurements were carried out in triplicates on samples diluted as needed in an aqueous 2% HNO_3 solution with the same NaCl concentration as the experimental fluids. The uncertainty of these analyses was generally lower than 2 %. Measurements of Na concentrations were also carried out using flame atomic absorption spectroscopy (AAS) using a Perkin Elmer AAnalyst 400 spectrometer. This technique proved to be more accurate than ICP-OES for the determination of Na concentrations.

Aqueous solution speciation calculations of the analyzed fluid samples were carried out using the geochemical code PHREEQC v. 3.7.0 (Parkhurst and Appelo, 2013) using the PSI/Nagra thermodynamic database (Thoenen et al., 2014) after addition of the thermodynamic constants of metal-borate complexes ($NaB(OH)_4^0$, $CaB(OH)_4^+$, $MgB(OH)_4^+$ and $SrB(OH)_4^+$) taken from the NIST46 database but originally derived from Smith and Martell (1989). Activity coefficients for the dissolved species were computed using the Davies equation embedded in this database. This choice was motivated by the reasonably accurate ion activity coefficients calculated by this model at seawater ionic strength (cf. Langmuir, 1997; Bethke et al., 2008) and by the necessity of having equilibrium calculations consistent with the surface complexation model (SCM) adopted in this study (see next section). The degree of saturation of the aqueous solutions relative to relevant solid phases, as calculated by PHREEQC, are expressed in terms of saturation indices (SI) according to:

$$SI=Log(IAP/K_{sp}) , \quad (1)$$

where IAP defines the ion activity product of the mineral hydrolysis reaction at the studied conditions and K_{sp} is the corresponding value of the solubility product. Alkalinity and pCO_2 were calculated by charge balance from measured element concentrations and pH assuming thermodynamic equilibrium of calcite (or aragonite) with each aqueous solution.

2.5 Boron adsorption modelling

Boron adsorption at the surface of calcite was modelled using the most recent and advanced surface complexation model developed by Heberling et al. (2021) for the calcite cleavage surface at equilibrium conditions. The model was refined after analysis and modelling of X-ray scattering (crystal truncation rod, CTR), inner surface potential (single-crystal electrode) and Zeta potential data, which allowed the accurate parametrization of a calcite three-plane model (TPM) describing the charge distribution and ion adsorption reactions occurring at the calcite-water interface in NaCl solutions. The development of the calcite TPM was based on PHREEQC, using the PSI/Nagra database for calculation of the equilibrium conditions, and took advantage of the tools provided by the Python programming language to build a dedicated graphical-user-interface-based software, P^{3}R (Python-PhreeqC-Parameter-Refinement), which was used to fit the experimental data and obtain the parameter values that define the SCM. The surface reactions with the corresponding formation constants and the adsorption parameters that define the calcite TPM are reported in Table 2. The reader is referred to the work by Heberling et al. (2021) for further details on the code and the parameter model calculations.

Within the formalism of the CD-MUSIC surface complexation approach (Hiemstra et al., 1989), the calcite TPM adopted in this study assumes the existence of two primary sites with fractional charge, $>CaOH^{-0.5}$ and $>CO_2O^{-0.5}$, the protonation of which can be described by the two following reactions occurring at the 0-plane:

$$>CaOH^{-0.5} + H^+ \leftrightarrow >CaOH_2^{+0.5} \quad (2)$$

and

$$>CO_2O^{-0.5} + H^+ \leftrightarrow >CO_2OH^{+0.5} \quad (3)$$

The reaction constants of the two surface protonation reactions were essentially determined by surface potential measurements and MUSIC calculations and have values corresponding to Log K_{CaOH} = 13.38 ±0.01 and Log K_{CO3H} = 1.3 ±0.1.The complexation reactions between the two primary surface species with Na^+, Cl^- and calcite constituent ions (Ca^{2+}, CO_3^{2-} and HCO_3^-) lead to the formation of different outer-sphere surface complexes. The binding constants of these ions with the calcite surface along with the corresponding charge distributions between the TPM planes are summarized by Heberling et al. (2021). The surface density of the Ca- and CO_3-sites were assumed to equal to 4.95 nm^{-2}, corresponding to the crystallographic site density of the (104) plane. Capacitance values for the inner and outer layer of the TPM were equal to 0.2 and 1.5 F/m^2, respectively. These capacitance values correspond to those provided by Heberling et al. (2021) for calcite and are within the narrow range (0.1-5 F/m^2) complying with the theoretical assumptions of SCM models (Heberling, 2025).

During the modelling of the adsorption data, it was assumed that borate ions could form two distinct surface complexes at the calcite-water interface: an inner-sphere complex formed by the substitution of $B(OH)_4^-$ for CO_3^{2-}; and an outer-sphere complex formed by adsorption of

$B(OH)_4^-$ on Ca-protonated sites. The formation of these surface species can be described by the following reactions occurring at the calcite-water interface:

$$> CO_3^{-0.5} + B(OH)_4^- \Longrightarrow > BO_3H_2^{+0.5} + HCO_3^- + OH^- , \quad (4)$$

$$\Delta z_0 = 0, \Delta z_1 = +1.0$$

$$> CaOH_2^{+0.5} + B(OH)_4^- \Longrightarrow > [CaOH_2^{+0.5} \cdots B(OH)_4^{-1}]^{-0.5} , \quad (5)$$

$$\Delta z_0 = 0, \Delta z_1 = 0, \Delta z_2 = -1.0$$

where $> BO_3H_2^{+0.5}$ and $> [CaOH_2^{+0.5} \cdots B(OH)_4^{-1}]^{-0.5}$ represent respectively the inner-sphere borate complex formed by surface ion-replacement and the outer-sphere surface species formed by simple adsorption of borate ions on protonated Ca-sites at the 2-plane of the TPM. The indicated values for Δz_0, Δz_1 and Δz_2 represent the corresponding change in charge distribution between the planes of the TPM (cf. Heberling et al., 2021). In reaction (4) the adsorption of $B(OH)_4^-$ involves a change of boron coordination from tetrahedral to trigonal geometry with partial deprotonation of the adsorbed borate, in agreement with the theoretical calculations and NMR data of boron coprecipitated with calcite (Mavromatis et al., 2015; Balan et al., 2016). The formation of the outer-sphere complex with a Ca-protonated site preserves the original tetrahedral geometry and defines a less strongly bound surface species. Note that the adsorption of boric acid was excluded on the basis of the evidence provided by Saldi et al. (2018), who showed that only $B(OH)_4^-$ ions are adsorbed from aqueous solutions by the calcite surface at equilibrium conditions.

Modelling of boron sorption on the aragonite surface was challenged by the absence of a SCM for aragonite and by the very limited data on surface charge distribution and sorption behavior relative to major ions. According to Zeta potential and surface charge measurements as a function of electrolyte concentration (Smallwood, 1977), calcite and aragonite show a similar behavior but the apparent adsorption capacity of both Ca and Mg ions is stronger on aragonite. In addition, aragonite naturally displays polar faces, such as {010}, {110} and {001} exposing either Ca-terminated or carbonate-terminated planes (Deer et al., 2013). Upon hydration these planes are stabilized (de Leeuw and Parker, 1998), or develop less polar or neutral microfacets, which are more stable in aqueous solution than the original polar faces (Kwak and Shindo, 2005). These properties of the aragonite surface make difficult to attribute an appropriate site density for Ca ions and CO_3 groups to model sorption reactions, considering also that the synthesized crystals are characterized by a complex micro-morphology (Fig. 2b). To overcome this complication it was decided to fix the surface site densities of Ca and CO_3 at the average crystallographic densities of {110} and {010} planes, in that these two planes are likely the most representative of our synthetic aragonite crystals. Based on this assumption, the calculated densities are equal to 3.61 and 5.47 nm^{-2} for Ca and CO_3 groups respectively. We finally assumed that the calcite SCM adopted in this study can describe with sufficient approximation aragonite surface chemistry and boron sorption reactions occurring on this mineral. Because boron incorporated into the aragonite structure is mostly present in tetrahedral coordination (Mavromatis et al., 2015; Balan et al., 2016, 2018), the formation of boron inner-sphere complex by substitution of a carbonate group can be better described by the following reaction:

$$> CO_3^{-0.5} + B(OH)_4^- + H_2O \Longrightarrow > BO_4H_4^{+0.5} + HCO_3^- + OH^-, \quad (6)$$

$$\Delta z_0 = 0, \Delta z_1 = +1.0$$

where the adsorbed $>BO_4H_4^{+0.5}$ species maintains the original coordination of aqueous borate. It can be noted that reactions (4) and (6) involve the same surface charge and the same charge balance, the only difference being in one additional water molecule associated to the inner-sphere complex of reaction (6). This difference does not affect the model calculations. As such, considering that the activity of H_2O can be assumed to be equal to 1, we can define a unique inner-sphere borate stability constant K_{B-IS} referring to either surface reaction.

The Python-based P^{3}R software (Heberling et al., 2021) was used in combination with the PhreeqPy tools working with PHRREQC to determine the intrinsic stability constants of reactions (4-6), and calculate the corresponding distribution of aqueous and surface species. The formation constants of the boron surface complexes defined above for calcite and aragonite are expressed by the following equations:

$$K_{B-is}^{int} = \frac{\{>BO_3H_2^{+0.5}\}\, a_{HCO_3^-}\, a_{OH^-}}{\{>CO_3^{-0.5}\}\, a_{B(OH)_4^-}} = \frac{\{>BO_4H_4^{+0.5}\}\, a_{HCO_3^-}\, a_{OH^-}}{\{>CO_3^{-0.5}\}\, a_{B(OH)_4^-}} \quad (7)$$

and

$$K_{B-os}^{int} = \frac{\{>[CaOH_2^{+0.5}\cdots B(OH)_4^{-1}]^{-0.5}\}}{\{>CaOH_2^{+0.5}\}\, a_{B(OH)_4^-}}, \quad (8)$$

where $\{i\}$ represents the concentration of the i*th* surface species and a_i stands for the activity of the subscripted aqueous species. Best-fit values of K_{B-is}^{int} and K_{B-os}^{int} were obtained by iterative simulations minimizing the difference between observed and modelled values via the chi-squared test method implemented in the program.

2.6 Measurements of boron isotopes

Prior to isotope ratio measurements, boron from experimental aqueous solutions was extracted from the samples through ion exchange chromatography, as detailed in Louvat et al. (2010). Basically, a volume of sample containing 500 ng of B was basified to pH 8-9 with ammonia (Suprapur, Merck). Chromatographic micro-columns were filled with 50 µL of the B-specific resin Amberlite IRA 743 previously ground and sieved between 100 and 200 mesh. Resin was washed with 15 mL of HNO_3 0.5 N, rinsed and conditioned with twice 0.2 mL of H_2O at pH 9 (DDI water basified with ammonia). Samples were loaded onto the resins, that were rinsed with 0.1 mL of H_2O at pH 9, 0.1 mL of $NaNO_3$ 0.6 M at pH 9, and again twice 0.1 mL of H_2O at pH 9. Boron was eluted from the resin with 0.05 mL of HNO_3 0.5 N and six times 0.1 mL of HNO_3 0.1 N. These boron fractions were then diluted to a volume of 2.5 mL in HNO_3 0.05 N. Blanks for the boron extraction procedure were between 0.5 and 1 ppb B, or 1.25 to 2.5 ng B. Given that the samples contained 500 ng of boron, these blanks, although high, represent less than 1% of the boron analyzed. The effect of this blank on the accuracy of the $\delta^{11}B$ measurement was tested by passing a seawater reference material (NASS-6) through columns every ten samples.

Boron isotope ratios were measured by MC-ICP-MS on a Nu1700 (Nu Instruments, UK) at IPREM - UPPA in Pau, using a 50 mL cyclonic spray chamber Peltier-cooled at 7°C, a 200 µL/min quartz micro-concentric nebulizer (micro-Mist, Glass Expansion), two Faraday cups equipped with 10^{11} Ohm amplifiers, "wet" high-sens skimmer (321-020) and sampler (319-285) nickel cones (Nu Instruments, UK). The sensitivity achieved was 5 V/ppm on ^{11}B. The

instrumental mass bias was corrected through sample-standard bracketing technique, using standard reference material NIST 951 (Catanzaro et al., 1970) at the same concentrations as the samples. Instrumental blanks were measured before each sample/standard and subtracted from the signals of the next sample/standard. Boron isotopic ratios were expressed in delta-notation ($\delta^{11}B$) relative to this standard according to: $^{11}B(‰) = \left[\left(\frac{^{11}B/^{10}B_{sample}}{^{11}B/^{10}B_{NIST\ 951}}\right) - 1\right] \times 1000$. The validity of the B isotope ratio measurements was assessed by the measurement of the reference materials AE120, AE121 and AE122 (BAM, Germany), for which we measured the following average values : –20.5 ± 0.9 ‰, 19.5 ± 0.7 ‰ and 39.3 ± 0.9 ‰ (2σ, n = 25), in full agreement with the reference values (Vogl and Rosner, 2011). The average measured $\delta^{11}B$ value for the seawater NASS-6 was 39.9 ± 0.7 ‰ (2SD, n = 6), in the range of the actual seawater value ($\delta^{11}B$ = 39.61 ± 0.04 ‰, 2SE, n = 28; Foster et al., 2010). Duplicate and triplicate measurements of some of the samples showed that the reproducibility cannot be claimed at better than 0.7 to 0.9 ‰, 2σ, consistent with that for the reference material multiple measurements.

2.7 Isotopic calculations

Adsorbed boron isotope composition ($\delta^{11}B_{ads}$) was deduced from the isotopic ratio measured in the aqueous samples ($\delta^{11}B_{sol}$) according to the following mass conservation equation:

$$\delta^{11}B_{ads} = \frac{\delta^{11}B_0 - \delta^{11}B_{sol} \cdot (1-X)}{X} \quad , \qquad (9)$$

where $\delta^{11}B_0$ represents the isotopic composition of the initial boron stock solution and X corresponds to the measured fraction of adsorbed B derived from aqueous solution analyses according to:

$$X = \frac{[B]_0 - [B]_{sol}}{[B]_0} \quad , \qquad (10)$$

where $[B]_0$ corresponds the concentration of boron at the beginning of each experiment and $[B]_{sol}$ is the boron concentration of the aqueous solution measured at the end of the experiment.

The boron isotope fractionation factor between the calcite or aragonite surface and the aqueous solution, $\alpha_{ads\text{-}sol} = \frac{(^{11}B_{ads})/(^{10}B_{ads})}{(^{11}B_{sol})/(^{10}B_{sol})}$, was calculated for each data point by the following expression (cf., Johnson et al., 2004; Saldi et al., 2018):

$$\alpha_{ads-sol} = exp\left(\frac{\delta^{11}B_{ads} - \delta^{11}B_{sol}}{1000}\right) = exp\left(\frac{\Delta^{11}B_{ads-sol}}{1000}\right). \qquad (11)$$

Modeling of experimentally determined fractionation factors was carried out starting from the calculated distribution of aqueous and surface species. Assuming that aqueous $B(OH)_4^-$ adsorbs at the $CaCO_3$/fluid interface giving rise to the formation of the two surface species defined by reactions (4) and (5), a fractionation factor for each surface complex with respect to aqueous boric acid can be defined according to:

$$\alpha_{4is-3sol} = \frac{(^{11}B/^{10}B)_{>BO_3H_2^{+0.5}}}{(^{11}B/^{10}B)_{B(OH)_3^0}} \qquad (12)$$

and

$$\alpha_{4os-3sol} = \frac{(^{11}B/^{10}B)_{>[CaOH_2^{+0.5}\cdots B(OH)_4^{-1}]^{-0.5}}}{(^{11}B/^{10}B)_{B(OH)_3^0}}. \quad (13)$$

The isotope ratios relative to the B adsorbed fraction ($R_{\text{B-ads}}$) and the corresponding aqueous counterpart ($R_{\text{B-sol}}$) can thus be expressed by the two following equations:

$$R_{B-ads} = \frac{\{>BO_3H_2^{+0.5}\}\cdot\alpha_{4is-3sol} + \{>[CaOH_2^{+0.5}\cdots B(OH)_4^{-1}]^{-0.5}\}\cdot\alpha_{4os-3sol}}{\{>BO_3H_2^{+0.5}\} + \{>[CaOH_2^{+0.5}\cdots B(OH)_4^{-1}]^{-0.5}\}} \quad (14)$$

and

$$R_{B-sol} = \frac{[B(OH)_3^0] + [B(IV)]_t\cdot\alpha_{4-3}}{[B(OH)_3^0] + [B(IV)]_t}, \quad (15)$$

where $\{i\}$ represents the concentrations of the i*th* boron surface species, $[i]$ stands for the concentration of the i*th* B aqueous species, and α_{4-3} is the boron isotopic fractionation factor between the aqueous borate ion and boric acid. Note that $[B(IV)]_t$ designates the total concentration of all tetrahedral B aqueous species: $B(OH)_4^-$ + $NaB(OH)_4^0$ + $CaB(OH)_4^+$ + $MgB(OH)_4^+$ + $SrB(OH)_4^+$.

The overall B isotopic fractionation factor between calcite/aragonite surfaces and the aqueous solution is given by the combination of the two previous equations, according to (cf. Lemarchand et al., 2007):

$$\alpha_{ads-sol} = \frac{R_{B-ads}}{R_{B-sol}} =$$

$$= \frac{\{>BO_3H_2^{+0.5}\}\cdot\alpha_{4is-3sol} + \{>[CaOH_2^{+0.5}\cdots B(OH)_4^{-1}]^{-0.5}\}\cdot\alpha_{4os-3sol}}{[B(OH)_3^0] + [B(IV)]_t\cdot\alpha_{4-3}} \cdot \frac{[B(OH)_3^0] + [B(IV)]_t}{\{>BO_3H_2^{+0.5}\} + \{>[CaOH_2^{+0.5}\cdots B(OH)_4^{-1}]^{-0.5}\}} \quad (16)$$

Modelled $\alpha_{\text{ads-sol}}$ values were deduced from the experimentally measured α values and the calculated distribution of B aqueous and surface species by a least square fitting of Eq. (16), using $\alpha_{4is-3sol}$ and $\alpha_{4os-3sol}$ as fitting parameters for a fixed value of α_{4-3}.

3. RESULTS

3.1 Boron adsorption on calcite in NaCl and ASW solutions

The results of the boron adsorption experiments conducted on calcite as a function of pH in ASW and NaCl 0.5 M aqueous solutions are reported on the plot of Fig. 3 and summarized in Tables 3-5. A typical bell-shaped adsorption envelope was observed for the NaCl 0.5 M aqueous solutions, with a minimum value of 7 nmol/m^2 and a maximum of 21 nmol/m^2 at pH 9.4-9.9, whereas a continuous increase of removed boron fraction with pH was observed for artificial seawater, ranging from 3 to 60 % (2-49 nmol/m^2). In Mg-poor ASW solutions removed boron fractions increased to intermediate values relative to NaCl and ASW solutions, reaching a maximum at pH 10.2-10.4 (31 nmol/m^2) and decreasing at higher pH.

For the experiments in ASW solutions Tables 4-5 also report the observed changes of concentrations for the other dissolved species (Na, Ca, K, Mg, Sr, SO_4), whereas all total dissolved inorganic carbon (TDIC) and log pCO_2 values were obtained from the corresponding

thermodynamic calculations. Significant changes in the concentration of dissolved seawater species were observed during the interaction of the aqueous solution with the calcite surface, excluding K and Na, for which the changes in concentrations were negligible. Ca concentrations were observed to decrease with increasing pH by ~11 to 34 % (see Table S3 for initial and final element concentrations of each experiment), whereas increasingly negative changes of Mg concentrations were recorded for pH ≥ 8.8, with a maximum decrease of –47 % at pH = 9.47 (Table 4 and S3). At pH < 8.8 the variation of Mg concentrations was close to or within the analytical uncertainty (< 7%). The experiments conducted in ASW showed also a systematic decrease of Sr concentration (52-64%) with respect to the starting ASW value, without any apparent pH-dependence. A similar behavior was observed for SO_4^{2-}, the concentrations of which decreased by 14-23 % relative to the initial concentration.

The results of thermodynamic calculations show that the ASW aqueous solutions were undersaturated with respect to the most relevant mineral phases, apart from calcite and aragonite, but approached equilibrium with respect to brucite ($SI_{Brc} > -0.5$) for pH > 9.1. (Table 4, Fig. S1).

In ASW with low Mg contents, the changes in Ca concentrations were more pronounced than observed in normal ASW, with variations that range from –66 to –78% (Table 4 & S4). The variations of Sr are on average comparable with those of normal ASW, whereas the differences of Mg concentration relative to the starting solution are comparable in relative terms to those reported for normal ASW. However, a slight increase in the measured Mg concentrations at pH < 9.7 can be seen. As in the case of normal ASW, measured Mg concentrations instead decreased with increasing pH, dropping dramatically when the aqueous solutions reached the equilibrium with brucite (Table 4).

3.2 Boron adsorption on aragonite in NaCl and ASW solutions

The results of boron adsorption on aragonite in ASW and NaCl solutions are illustrated on the plot of Fig. 4 and reported in Tables 6-7. The B removal behavior is similar to that observed for calcite but the measured extents of adsorption are 2-4 times higher than for calcite, reaching an adsorbed amount of 67 nmol/m^2 (pH = 9.09) in NaCl medium and a maximum of 111 nmol/m^2 in ASW, where only a fraction of boron can be explained by adsorption at pH > 9. Boron adsorption increases monotonically with increasing pH in ASW whereas it appears to replicate the same dependence on pH as calcite in NaCl 0.5 M with a maximum adsorption between pH 9 and 10 and decreasing extent of adsorption at more basic conditions.

As observed for calcite, Ca concentrations showed a continuous decrement relative to the starting ASW composition with increasing pH. The only increment (+11 %) was measured at pH = 7.54 (expt. BS-08). No appreciable variation of Mg concentration was observed, except for the experiment at pH 9.5 (–6 %; Table S5), whereas the other significant changes in concentrations were measured for Sr (–14 to –21%). Both K and SO_4^{2-} showed systematic decreases in concentration but such variations (–1 to – 8%) were mostly within the analytical errors of the two elements. According to thermodynamic calculations, the ASW solutions equilibrated with aragonite became saturated with respect to brucite at pH > 9.3 (Table 7). The precipitation of this phase might be responsible for the small decrease in aqueous Mg concentration observed in these solutions.

3.3 Boron removal from $CaCO_3$-free suspensions

The effects of NaOH additions to seawater on dissolved boron concentration was assessed with experiments devoid of calcite or aragonite powder, where 4 different volumes of NaOH 1M were added to ASW before (experiments BM) and after (experiments BQ) boron was added to the aqueous solution. Additions of the indicated volumes of base provoked the formation of a cloudy suspension or the almost immediate precipitation of a solid made of very fine particles, as observed by visual inspection. The formation of this solid phase coincided with a marked decrease of Mg, Ca and K. This process was accompanied by a significant decrease of dissolved boron concentrations (Δ[B]) with differences ranging from –0.3 to –2.7 ppm relative to the initial concentration, which correspond to extents of B adsorbed or co-precipitated of 6-50 % (Table 8). The white precipitate collected from the BQ-series was analyzed by X-ray powder diffraction and resulted to be composed mainly of brucite with a tiny amount of calcite (Fig. 5). Thermodynamic calculations on the 8 aqueous samples withdrawn from these experiments show that these aqueous solutions are from slightly undersaturated to weakly oversaturated relative to brucite, depending on the assumption made to fix or calculate the corresponding pCO_2 (initial equilibrium with atmospheric pCO_2, before NaOH addition, pCO_2 = constant = $10^{-3.4}$ bar or equilibrium with respect to calcite). The SSA_{BET} measured on the precipitated solid (< 0.1 g) recovered from the experiments of the BQ-series provided a lumped value of 56.0 m^2/g.

3.4 Boron adsorption modelling

3.4.1 Boron adsorption on calcite

The formation constants of the two B surface species (Eq. 7 and 8) that provide the best fit of the experimental data are reported in Table 9. It has to be noted that when modelling boron adsorption in ASW we excluded the data at pH > 8.8. Because these alkaline solutions show a significant change in Mg concentration (> 8 %) and gradually approach the equilibrium with respect to brucite (Fig. S1), the apparent increase in B adsorption might be affected by these chemical changes. Modelling of the adsorption data obtained in NaCl 0.5 M over the entire range of pH results in intrinsic stability constants of B inner-sphere and outer-sphere complexes that are respectively 0.7 and 1.4 log units higher than the values calculated by modelling of the seawater data. This translates to an apparently higher fraction of adsorbed B and a bigger proportion of outer-sphere B complex in NaCl solutions compared to ASW. The comparison between boron adsorption data and the corresponding values calculated by the model for NaCl and ASW solutions is illustrated on the plot of Fig. 6.

Two alternative models were also tested, in which either the inner-sphere or the outer-sphere were the only borate complex forming by the adsorption reaction. In each case, the agreement between calculated and measured boron data was poorer and, consequently, the formation of a single surface species was not considered as plausible as the formation of the two distinct borate surface complexes.

3.4.2 Boron adsorption on aragonite

B adsorption on aragonite in NaCl and ASW solutions was interpreted using the same model assumption as calcite. As in the case of calcite, the determination of the two B adsorption constants did not take into account the data acquired at more alkaline conditions (pH > 8.8). Although the changes in Mg concentration for pH > 8.8 are close to or within the analytical uncertainty, these aqueous solutions were found to be at equilibrium with brucite, which might

have affected the resulting boron concentrations. The results of the modelling study are summarized in Fig. 7 and Table 9. The formation constant of the inner-sphere borate complex, K_{B-is}^{int}, is 2 and 6 times higher than determined for calcite, whereas the fitted values of K_{B-os}^{int} are, respectively, 8 and more than one thousand times higher in NaCl 0.5 M and ASW. We also note that, according to the TPM, the proportion of the outer-sphere B complexes is bigger than borate inner-sphere complex and higher in ASW than in NaCl 0.5 M, as opposed to calcite where the borate inner-sphere complex is the dominant adsorbed species, particularly in seawater (see the corresponding stability constants of each surface complex in Table 9).

3.4 Boron isotopic data

The isotopic composition of the fluid samples collected from the adsorption experiments ($\delta^{11}B_{sol}$), the calculated compositions of adsorbed boron ($\delta^{11}B_{ads}$) and the corresponding values of boron isotope fractionation factor between the carbonate surface and the aqueous solution, $\alpha_{ads-sol}$, are listed in Tables 10 and 11. Considering the uncertainties of the analyses, the measured B isotopic composition of the two starting solutions is the same ($\delta^{11}B_0$= –0.09 ±0.1 for NaCl 0.5 M; $\delta^{11}B_0$= –0.02 ±0.27 for ASW). The isotopic fractionation factors obtained from the analyses of the aqueous samples according to Eq. (11) are plotted as a function of pH in Fig. 8. The B fractionation factors between the calcite surface and the aqueous solutions exhibit similar behavior in NaCl 0.5 M and ASW at pH < 9.2, with $\alpha_{ads-sol}$ values that range between 0.963 and 0.997 (-38 ‰ ≤ $\Delta^{11}B_{ads\text{-}sol}$ ≤ -3.0 ‰). At higher pH values the two datasets diverge. The B fractionation factors relative to ASW increase steeply with pH, due to B adsorption and coprecipitation with brucite, reaching a value of $\alpha_{ads-sol}$ = 1.011 at pH = 9.47, whereas the α-values obtained from NaCl 0.5 M solutions increase more gradually up to a maximum of 1.005 ($\Delta^{11}B_{ads\text{-}sol}$ = +4.7 ‰) at pH 10.3 (Fig. 8a).

The boron isotopic fractionation between aragonite and the aqueous solution is apparently less pronounced than observed in the case of calcite. Boron fractionation factors (Table 9, Fig. 8b) vary within a range of 0.980 - 1.002 (-20.0 ‰ ≤ $\Delta^{11}B_{ads\text{-}sol}$ ≤ +2.2 ‰), if we exclude the lowest measured value ($\alpha_{ads-sol}$ = 0.954), which is affected by large uncertainties due to the smallest amount of B adsorbed (~ 4 %).

The variation of B fractionation factor with pH in NaCl solutions mimics the corresponding change of $B(OH)_4^-$ isotopic composition (cf. Lemarchand et al., 2005 ; Saldi et al. 2018), which is described by the dashed line on the plots of Fig. 8a-b, calculated for a fractionation factor value between $B(OH)_4^-$ and $B(OH)_3^0$, α_{4-3}, equal to 0.9735 (Klochko et al., 2006) and an apparent dissociation constant of the boric acid ($Log\ K_B$) equal to –8.99, as calculated by PHREEQC using the PSI/Nagra database.

The two plots of Fig. 8 also show the fractionation factor of boron associated with brucite precipitation for the experiment BQ-8, corresponding to the highest amount of base added to seawater and the highest fraction of boron taken by the precipitate. As in the case of calcite and aragonite, the isotopic composition of the boron associated to the solid phase is slightly heavier than the composition of the borate aqueous ion.

3.5 Modelling of B isotopic fractionation between $CaCO_3$ surface and aqueous solution

The isotopic fractionation of $B(OH)_4^-$ between the assumed borate surface complexes and the aqueous solution has been determined by modelling of the overall fractionation factors ($\alpha_{ads-sol}$) calculated with Eq. (11). The values of the fractionation factors of the inner-sphere

species and the outer-sphere complex relative to boric acid, $\alpha_{4is-3sol}$ and $\alpha_{4os-3sol}$, were fixed by a least-square fitting method using Eq. (16) for α_{4-3} = 0.9735. This value corresponds to the fractionation factor between boric acid aqueous borate proposed by Klochko et al. (2006) for artificial seawater (α_{3-4}= 1/α_{4-3} = 1.0272), which was adopted in our previous study (Saldi et al., 2018) of boron adsorption on calcite in more dilute solutions (0.01 and 0.1 M NaCl). Note that Nir et al. (2015) proposed a fractionation value of 26.0 ±1.0 ‰ between boric acid aqueous borate. This is sometimes preferred to the value of Klochko et al. (2006) but it is within uncertainty the same.

The fractionation factors of the two borate surface species calculated for both calcite and aragonite are reported in Table 9. Borate adsorbed on calcite is heavier than its dissolved counterpart in both NaCl 0.5 M ($\alpha_{4is-3sol}$= 0.9812, $\alpha_{4os-3sol}$=0.9782) and ASW solutions ($\alpha_{4is-3sol}$= 0.9782). Note that we did not attribute any value to $\alpha_{4os-3sol}$ for calcite in seawater because the predicted concentrations of the outer-sphere complex are negligible (< 0.5 %) compared to the overall adsorbed boron. As such, the formation of this complex had no appreciable impact on the fitted results. Similar fractionation values were also obtained for aragonite inner-sphere species ($>BO_3H_2^{+0.5}$ or $>BO_4H_4^{+0.5}$) even if they were derived from fewer datapoints in NaCl solutions and, therefore, are less constrained than for calcite. The outer-sphere complex ($>[CaOH_2^{+0.5}\cdots B(OH)_4^{-1}]^{-0.5}$) adsorbed on aragonite in NaCl 0.5 M solutions has the same isotope fractionation as dissolved borate, whereas it is heavier than the dissolved form in ASW (enriched in ^{11}B by 3.7‰).

The comparison between the measured overall fractionation factors ($\alpha_{ads-sol}$) and the corresponding curves obtained from the α-values determined for the two adsorbed B species is illustrated in the plots of Fig. 9 and 10. For calcite, the calculated curves are in very good agreement with the experimental data, showing an overall fractionation between adsorbed borate species and aqueous $B(OH)_4^-$ that varies with pH between 6.2 and 7.5 ‰ in 0.5 M NaCl solutions, depending on the relative abundance of the two surface species, and is constant and equal to 4.7 ‰ in ASW (only $>BO_3H_2^{+0.5}$ contributes to the measured fractionation factors). The fractionation factors of adsorbed borate species vary in a different fashion for aragonite, showing a roughly constant fractionation between adsorbed and dissolved borate ion in artificial seawater (~ 4.1 ‰) and a fractionation that gradually decreases from 4.1 ‰ at pH 7 to 1.2 ‰ at pH 12 in NaCl solutions, following the increasing concentration of the outer-sphere complex with pH.

4. DISCUSSION

4.1 Differences in boron adsorption behavior between calcite and aragonite and the effect of dissolved Mg

It is evident from our experimental measurements and modelling results that the adsorption of boron on aragonite in seawater is stronger and increases more rapidly with pH than for calcite. This observation is consistent with the stronger affinity of $B(OH)_4^-$ for the aragonite structure, as shown by studies reporting on the B coordination within the structure of calcite and aragonite and its partitioning during co-precipitation with the two polymorphs (Sen et al., 1994; Mavromatis et al., 2015; Balan et al., 2016). The surface complexation model adopted to describe the adsorption of the borate ion at the $CaCO_3$-fluid interface clearly illustrates the preference of $B(OH)_4^-$ for the aragonite surface, as the formation constants of the two borate complexes are at least two times higher with respect to calcite. Despite the uncertainties inherent in the application of the calcite TPM to aragonite, the modelling results

show also a different distribution of $B(OH)_4^-$ surface complexes compared to calcite. While the surface complex formed by substitution of CO_3 groups ($> BO_3H_2^{+0.5}$) is the dominant species adsorbed on calcite (> 90 %), the adsorbed outer-sphere complex formed on the Ca-sites of aragonite ($> [CaOH_2^{+0.5} \cdots B(OH)_4^{-1}]^{-0.5}$) is more abundant (> 79 %) than the inner-sphere complex over the studied pH range only in seawater. Conversely, in NaCl solutions, the outer-sphere complex formed on the aragonite surface is less abundant than the inner-sphere surface complex, accounting for 10-55 % of total adsorbed boron.

The values of the intrinsic constant of formation of the two borate surface complexes reported in Table 9 suggest that boron adsorption in ASW on both calcite and aragonite is weaker than in NaCl solutions, although the decrease of the intrinsic stability constant of the inner-sphere complex for aragonite is partially compensated by the increase of the intrinsic equilibrium constant of the outer-sphere complex. Because there is no significant difference in the adsorption behavior between the two aqueous solutions within the modelled pH range (see Figs. 3 and 4), the difference of intrinsic constant values seemingly stems from the incomplete account by the TPM of the surface charge effects related to the presence of foreign ions, namely Mg^{2+} and SO_4^{2-}, which interact with the $CaCO_3$ surface in seawater. The application of the same surface complexation model to the boron adsorption data reported by Saldi et al. (2018) for calcite in more dilute solutions (NaCl 0.01 M; Table 9) results in values of the two intrinsic constant of borate surface complex formation that are intermediate between those determined for ASW and NaCl 0.5 M, showing that the uncertainties associated to the intrinsic constant values are, however, in the range of 0.2-0.4 log units.

In modelling the adsorption of borate in ASW we excluded the data that were likely affected by the precipitation of brucite, because the formation of this phase could be responsible for the adsorption/coprecipitation of a fraction of dissolved boron. This hypothesis is supported by our experiments of B adsorption and coprecipitation in artificial seawater (Table 8) without calcite and aragonite. Our results suggest that brucite can scavenge a considerable amount of boron compared to the two $CaCO_3$ polymorphs. Based on the data reported in Table 8, we can estimate the boron partition coefficient, K_d, between brucite and ASW and compare it with those relative to the adsorption on calcite and aragonite. The partition coefficient of boron between the solid phase and the aqueous solution is expressed by:

$$K_d = \frac{(m_{B-ads}/m_{solid})}{(m_{B-aq}/m_{solution})} \ , \qquad (17)$$

where m_{B-ads}, m_{B-aq}, m_{solid} and $m_{solution}$ correspond to the respective masses of adsorbed or coprecipitated boron, dissolved boron, solid and aqueous solution.

Mass balance calculations of magnesium indicate that between 9 and 36 mg of $Mg(OH)_2$ formed prior to adsorption of boron on this precipitate. According to the measured changes of B concentration this translates into K_d values of 189-295 for adsorption (BM series), whereas for the boron co-precipitated with brucite K_d increases to 697-908 (BQ series). These partition coefficients are in good agreement with those reported by Xiao et al. (2011) for boron incorporation in brucite during precipitation from artificial seawater. The authors determined K_d of 360-494 after experiments at pH of 9.5-10.0. The partition coefficients for adsorption onto calcite and aragonite in ASW with negligible change of Mg concentration (pH < 8.8) vary between 0.1 and 1.4. This comparison indicates that even the very small amount of brucite forming during $CaCO_3$ equilibration in seawater at more basic pH can significantly enhance the removal of boron from the aqueous solution. According to our thermodynamic calculations, however, not all the aqueous solutions characterized by a significant decrease of Mg

concentration (> 5-7 %) and a higher extent of B adsorption relative to NaCl solutions were at or close to equilibrium with respect to brucite (Tables 4, 5 and 7). This suggests that $B(OH)_4^-$ adsorption at the calcite/aragonite surface might partly occur via the binding of borate ion pairs, such as $MgB(OH)_4^+$, or might be enhanced by the interaction of the $CaCO_3$ surface with Mg^{2+} and other ions, without the formation of brucite or other secondary phases incorporating some fraction of dissolved boron. It is well-known that Mg exchanges for Ca on the calcite surface (cf. Davis et al., 1987) or competes with other cations for adsorption sites in seawater (e.g., Mucci and Morse, 1983; Franklin and Morse, 1983; Kornicker et al., 1985), whereas the interaction of Mg^{2+} with the aragonite surface is much more limited (cf. Gabitov et al., 2008; Mavromatis et al., 2022). Because of the relative abundance of $MgB(OH)_4^+$ compared to the other aqueous borate complexes (Fig. S3), the high charge density of Mg^{2+} and its specific interaction with the calcite surface, this ion pair could be adsorbed at the negatively charged calcite surface (cf. Heberling et al., 2011, 2021), increasing the total amount of adsorbed borate. This hypothesis was recently made to explain the adsorption of boron on clay minerals in seawater within the pH-range of modern oceans and above (Ring et al., 2025). In our case, this reaction could take place at $8.7 \leq pH_{NBS} \leq 9.1$, where the extent of B adsorption is apparently higher than in Mg-free solutions and the saturation indices of the fluid with respect to brucite should not allow for its precipitation ($SI_{Brc} < -0.6$). The possible contribution of this reaction is, however, difficult to assess because of the lack of data on Mg adsorption reaction and the difficulty of distinguishing adsorption from precipitation at more alkaline pH.

According to the adsorption data distribution for aragonite (Fig. 4) and given the limited interaction of Mg^{2+} with this mineral surface, the contribution of ion pairs to the adsorption of $B(OH)_4^-$ is presumably less important than for calcite but cannot be excluded a priori. However, the higher masses of boron adsorbed on aragonite at pH > 9 can be related to the precipitation of small amounts of brucite as these fluids are essentially saturated or slightly supersaturated with respect to this phase.

4.2 Changes in seawater dissolved ion concentrations and isotopic composition of B adsorbed species

The distribution and isotopic composition of the $B(OH)_4^-$ surface complexes formed in seawater on calcite and aragonite show some remarkable differences compared to NaCl solutions, which can originate from the interaction of other aqueous species with the carbonate surface during the equilibration and adsorption processes.

During reaction of calcite with ASW we can note a net decrease of Ca^{2+}, SO_4^{2-} and Sr^{2+} concentrations. Changes of Ca concentration vary between 46 and 131 ppm (a decrease of 11-34 % relative to the starting ASW concentration; Table S3) following a weakly negative pH-dependence. Such decrease might be somewhat unexpected considering the initial condition of undersaturation of the aqueous solutions with respect to calcite, but it is likely the result of the equilibration at relatively low pCO_2 and high alkalinity of the equilibrated seawater solutions, revealing the possible re-precipitation of calcite or less soluble Mg-calcite with increasing pH (cf. Mucci and Morse, 1984) before or after boron addition to the suspensions. In this case, however, the amount of precipitated calcite would be so limited (< 0.01 g) that it could not affect boron adsorption. The decrease of Ca concentration in the Mg-poor ASW solutions is stronger than in normal ASW, but also in this case the corresponding amount of calcite precipitated (< 0.02 g, less than 0.3 % of the initial calcite mass) could not affect the extent of boron adsorption and the isotope composition of the dissolved fraction. Aqueous SO_4^{2-} decrease reflects a significant adsorption of this ion on the calcite surface. The extent of sulfate adsorption (590-900 nmol/m^2) is more than 10 times larger than measured for boron. The

differences of Sr concentration with respect to the initial ASW range between 1.1 and 2.6 ppm and correspond to adsorption amounts of 6-8 nmol/m^2, which are comparable to those measured for boron at pH< 8.

Looking at our data, the interaction of SO_4^{2-} and Sr^{2+} with the calcite surface does not seem to significantly impact boron adsorption and isotopic fractionation in ASW relative to the NaCl aqueous solution (Figs. 3 and 8a), at least at the conditions where boron adsorption is not affected by the presence of dissolved Mg (pH < 9). Nonetheless, modeling of boron adsorption data and isotope fractionation factors between the calcite surface and the fluid indicates that the borate inner-sphere species formed at the calcite surface in seawater is ~3 ‰ lighter than the same surface complex in NaCl 0.5 M. This can be related to the distortion of the calcite surface structure by adsorbed sulfate anions which, substituting for the smaller planar CO_3 groups, likely modify the bonding environment of borate ions. This interpretation is consistent with the isotopic composition of boron co-precipitated with calcite in phosphate- and sulfate-bearing solutions (Uchikawa et al., 2023). These authors observed an increase in the B/Ca ratio and a decrease of calcite $\delta^{11}B$ by 1.9 and 2.8 ‰ compared to reference aqueous solution ($CaCl_2$-$NaCO_3$ fluid at pH ~ 8.2) when 2 and 5 mmol of Na_2SO_4 were respectively added to the growth solution. SO_4^{2-} ions were also observed to impact the partition coefficient and isotopic composition of Mg incorporated during Mg-calcite precipitation (Goetschl et al., 2019; Mavromatis et al., 2025), highlighting the role of solution composition on the distribution and isotope fractionation of trace elements taken up by precipitating calcium carbonate polymorphs.

The changes in concentration of SO_4^{2-} and Sr^{2+} during the interaction of ASW with aragonite show that both ions have a stronger affinity with the aragonite surface compared to calcite. Measured Sr concentrations indicate that its adsorption increases with increasing pH from ~10 nmol/m^2 (pH = 7.5) to 20-25 nmol/m^2 (pH =9.5), whereas SO_4^{2-} adsorption varies between 300 and 1500 nmol/m^2 within the same pH interval, but without an apparent dependence on this parameter. The higher affinity of Sr^{2+} for the aragonite orthorhombic structure compared to the calcite structure is well documented in the literature (cf. Zhong and Mucci, 1989; Dietzel et al., 2004; Sunagawa et al., 2007; Brazier et al., 2023). In contrast, SO_4^{2-} generally exhibits higher concentrations in calcite (Busenberg and Plummer, 1985; Fernández-Díaz et al., 2010; Bots et al., 2011; Barkan et al., 2020). Regardless of the preference of these ions for one or the other polymorph, their interaction with the carbonate surface at seawater-like concentrations can significantly modify the lattice parameters of these minerals (Staudt et al., 1994; Pingitore et al, 1995; Kontrec et al., 2004; Fernández-Díaz et al., 2010; Okumura et al., 2018; Barkan et al., 2020) and affect the B-O bond length and isotopic composition of $B(OH)_4^-$ adsorbed at the $CaCO_3$ surface. The adsorption of $B(OH)_4^-$ on the aragonite surface shows even more pronounced differences between NaCl solutions and artificial seawater than calcite. This is reflected by the isotopic compositions of the corresponding surface complexes. Our modelling results suggest that $B(OH)_4^-$ adsorption at the aragonite-water interface in NaCl 0.5 M involves the formation of an inner-sphere species enriched in the heavy isotope (+4.2 ‰) together with an outer-sphere complex with the same isotope composition as dissolved borate. The combination of these two borate surface species results in adsorbed $B(OH)_4^-$ that is 4.1 to 1.2 ‰ heavier than the aqueous borate at $7.0 \leq pH \leq 12.0$, as the concentration of the unfractionated complex increases with increasing pH. In ASW solutions both the borate inner-sphere ($>BO_3H_2^{+0.5}$) and the outer-sphere ($>[CaOH_2^{+0.5}\cdots B(OH)_4^{-1}]^{-0.5}$) complexes exhibit a heavier composition compared to NaCl solutions (Table 9) leading to an overall isotope composition of adsorbed boron that is 4.1-4.3 ‰ heavier than aqueous borate. At typical seawater pH values (8.1-8.2) this translates into fractionation factors ($\Delta^{11}B_{ads-sol}$) of 4.0-4.1 ‰ in NaCl 0.5 M and 5.4-6.5 ‰ in ASW. This suggests that the incorporation of SO_4^{2-}, and

possibly Mg^{2+} and Sr^{2+}, in the aragonite surface structure affects the isotope composition of adsorbed borate, but acts in the opposite direction compared to calcite, that is, by favoring the formation of slightly heavier B surface complexes than in NaCl solutions.

It was suggested that changes in the isotopic composition of boron taken up by $CaCO_3$ during growth in seawater may result from the incorporation of ion pairs ($CaBOH_4^+$, $MgBOH_4^+$) with slightly different isotopic composition (Henehan et al., 2022), the adsorption/incorporation of which across a negative surface potential would be facilitated by their positive charge. Although it is difficult to provide an estimate of the boron fraction that could be adsorbed as BOH_4^--complexes, their isotopic composition should not differ significantly from that of borate. Recent first-principle estimates of the isotopic composition of aqueous $NaBOH_4°$, $CaBOH_4^+$ and $MgBOH_4^+$show that these complexes are no more than 1 ‰ heavier than the free borate ion (Yin et al., 2023). So, even if a sizeable fraction of borate ion pairs was involved in the adsorption process, the effect on the isotopic composition of adsorbed boron should be negligible.

4.3 Implications for understanding the mechanisms of incorporation of boron in marine carbonates and the resulting fractionation factors.

The results of this study show that borate ions adsorbed both on calcite and aragonite surfaces exhibit a different isotopic composition relative to their aqueous counterpart. The observed $B(OH)_4^-$ fractionation between calcite surface and NaCl 0.5 M aqueous solution is consistent with that measured in more dilute NaCl solutions (Saldi et al., 2018) and reflects, at least in part, the isotopic composition acquired by boron during various inorganic coprecipitation experiments (Sanyal et al., 2000; Noireaux et al., 2015; Farmer et al., 2019). The isotope fractionation factors for boron adsorbed species in NaCl solutions are slightly higher than those measured in artificial seawater, suggesting that the interaction of the calcite surface with other dissolved ions (particularly SO_4^{2-}) affects the structure of the mineral surface favoring the adsorption of lighter borate relative to NaCl solutions.

Measured B isotope fractionation between aragonite surface and NaCl solutions, based on few datapoints, is, within the uncertainties, very close to the fractionation between aqueous borate and boric acid (Fig. 10a), which is consistent with the data reported by studies of boron incorporation during aragonite inorganic precipitation (e.g., Noireaux et al., 2015; Henehan et al., 2022) and what is generally assumed according to the paleo-pH proxy hypotheses. In addition, the results of the three-plane model show that the adsorption of $B(OH)_4^-$ at Ca-protonated sites occurs without isotopic fractionation between the aragonite surface and the aqueous solution. This suggests that the incorporation of boron during aragonite growth in NaCl solutions at close-to-equilibrium conditions should be controlled by borate adsorption at these surface sites.

In seawater solutions, borate complexes adsorbed on the aragonite surface display a clear enrichment in ^{11}B relative to dissolved borate (Fig. 10b). The measured B-isotope fractionation qualitatively agrees with the isotope composition of various biogenic aragonite samples showing a preferential incorporation of the heavier isotope relative to seawater borate ion (e.g., Hönisch et al., 2004; Reynaud et al., 2004; Krief et al., 2010). It is known that the pH of the calcifying fluids is generally higher than that of seawater (e.g., Trotter et al., 2011; Venn et al., 2013; Holcomb et al., 2014), which favors the incorporation of $B(OH)_4^-$ ions that are isotopically heavier than in seawater but presumably not fractionated with respect to the borate composition of the internal fluid. However, the isotopic composition of biogenic aragonite might also be controlled by boron adsorption on a surface distorted by the incorporation of trace

elements, such as sulfate, and not the result of vital effects, fluid pH changes in the vicinity of the calcifying organisms or the possible incorporation of boric acid (cf. Rollion-Bard et al., 2011; Chalk et al., 2021). The verification of this hypothesis would require investigation of B isotopic behavior during abiotic aragonite coprecipitation from seawater solutions and the comparison with the boron isotope composition of biogenic aragonite cultures obtained under controlled conditions of pH and composition of the calcifying fluid (cf. Comeau et al., 2017; Le Goff et al., 2017).

By comparing the results of studies that synthesized aragonite from seawater (Holcomb et al., 2016; Alvarez et al., 2024) with the data from inorganic studies in SO_4-free Na-Ca-Mg-Cl aqueous solutions (e.g., Noireaux et al., 2015; Henehan et al., 2022), it seems likely that the presence of SO_4^{2-} can increase the B/Ca ratio of precipitated aragonite crystals. As shown by Uchikawa et al. (2023), the incorporation of SO_4^{2-} during calcite growth, possibly combined with other ions or aqueous complexes, leads to an increase of the B/Ca ratio inducing a significant change of B isotope composition relative to NaCl solutions. An analogous effect might be observed for the borate ions incorporated during aragonite growth in seawater. The resulting B isotope fractionation should help understand the control of aragonite surface structural changes on the isotopic composition of coprecipitated boron and the extent to which its incorporation is consistent with $B(OH)_4^-$ adsorption at crystallographic sites versus growth controlled by surface kinetic effects (cf. Farmer et al., 2019).

5. CONCLUDING REMARKS

Boron adsorption on calcite and aragonite was measured in artificial seawater and NaCl solutions of the same ionic strength (0.5 M) and was modelled using the calcite three-plane model (TPM) developed by Heberling et al. (2011, 2021) assuming the presence of an inner-sphere $B(OH)_4^-$ complex, formed by substitution of a surface carbonate group ($>BO_3H_2^{+0.5}$ or $>BO_4H_4^{+0.5}$), and the binding of $B(OH)_4^-$ to Ca-protonated sites ($>[CaOH_2^{+0.5}\cdots B(OH)_4^{-1}]^{-0.5}$) at the 2-plane of the TPM. The stronger adsorption of $B(OH)_4^-$ on the aragonite surface compared to calcite is explained by the higher fraction of both borate surface complexes in NaCl solutions. In seawater solutions the outer-sphere complex becomes the dominant borate species adsorbed on aragonite ($>[CaOH_2^{+0.5}\cdots B(OH)_4^{-1}]^{-0.5}$ > 79%), but is negligible (<1 %) relative to the inner-sphere complex on the calcite surface.

The analysis of the boron isotopic composition indicates that adsorbed $B(OH)_4^-$ is enriched in the heavy isotope relative to the composition of aqueous borate for both calcite and aragonite, with overall enrichments of 4.7-7.5‰ and 1.2-4.1‰, respectively. The two borate surface complexes exhibit different isotopic fractionation factors, which, considering the data of Saldi et al. (2018) at I = 0.01 M, vary with the ionic strength and the composition of the aqueous solution for both $CaCO_3$ polymorph. The B isotopic composition of the inner-sphere complex formed on calcite in NaCl solutions at 0.5 M is ~4.9‰ heavier than in more dilute solutions (NaCl 0.01 M), but ~3 ‰ lighter in artificial seawater compared to NaCl 0.5 M solutions. The composition of the outer-sphere complex on calcite is, within the uncertainties, the same in both NaCl solutions but could not be determined in seawater because of its very low concentration.

Boron adsorbed at the aragonite/fluid interface showed different isotope fractionations between NaCl 0.5 M and artificial seawater. The outer-sphere complex resulted to be ~ 3.7‰ heavier in ASW than in NaCl solutions, whereas the inner-sphere complex was only slightly enriched in ^{11}B (+0.5‰) compared to NaCl solutions. The reported changes in isotopic

composition of the borate surface complexes formed in seawater could originate from the earlier adsorption of SO_4^{2-}, which was also observed to affect the isotopic composition of boron co-precipitated with calcite via modification of the crystal lattice structure (see Uchikawa et al., 2023).

The first isotopic measurements of boron adsorbed on aragonite here reported partially contradict the predictions of the paleo-pH proxy tool as well as the data from inorganically precipitated aragonites (Noireaux et al., 2015; Henehan et al., 2022), but is in fair agreement with the data on aragonite and calcite formed via an ACC pathway (Mavromatis et al., 2021) and from first principle calculations (Balan et al., 2018; Yin et al., 2023). The disagreement with the results from classical crystal growth experiments calls for more accurate measurements of boron isotope fractionation during coprecipitation with aragonite in seawater via different pathways and at different degrees of saturation. It is not known to what extent seawater composition can affect the boron isotope composition of precipitating aragonite, but our results should provide useful information to identify the prevailing mechanisms controlling the $\delta^{11}B$ values acquired during the growth process.

From a more general standpoint the present study highlights the control of surface chemical speciation and mineral/water interface structure on the isotopic fractionation associated with the adsorption of aqueous ions on carbonate minerals. Although the calculated isotopic composition of surface complexes is model-dependent, changes of ionic strength, aqueous solution composition and bonding environment are critical in determining the isotopic composition of aqueous species adsorbed at the $CaCO_3$ surface and their effects deserve more detailed studies.

Acknowledgements

The work received the financial support from the French national program LEFE/INSU and the French Agency of Research (ANR) through the research project "MeLiCa" (ANR-22-CE01-0001-04). We thank Carole Causserand and Philippe Besson for the technical assistance during ICP-OES analyses and Alain Castillo for helping with BET specific surface area measurements. We are grateful to Ludovic Menjot and Jean-Michel Brazier for their help with XRD analyses and aragonite synthesis. We also thank Stéphane du Plouy and Teresa Hungria at the Raimond Castaing Micro-characterization Center in Toulouse for their help and assistance during SEM-EDX and TEM analyses of the solid samples. GDS expresses his gratitude to Guntram Jordan for the insightful discussions during the interpretation of the experimental data. Finally, we thank Michael Henehan, Mario Villalobos and two anonymous reviewers for their constructive comments, which helped improve the original manuscript. Editorial handling by Mario Villalobos is gratefully acknowledged.

Data Availability

Data are available through Mendeley Data at: DOI.10.17632/wtmfycppd8.1

Appendix A. Supplementary Material

It includes: (i) tables summarizing the experimental conditions and reporting the initial and final concentrations of the elements dissolved in artificial seawater; (ii) plots illustrating the isotopic composition of adsorbed/coprecipitated boron and the distribution of dissolved borate

complexes with seawater pH; and (iii) illustration of the change in Mg concentration in ASW with increasing pH and increasing brucite saturation.

CRediT authorship contribution statement

Giuseppe D. Saldi: Conceptualization, Methodology, Formal analysis, Investigation, Data curation, Validation, Visualization, Writing – original draft, Writing – review & editing. **Pascale Louvat:** Conceptualization, Formal Analysis, Investigation, Methodology, Validation, Writing – review & editing. **Frank Heberling:** Conceptualization, Formal Analysis, Investigation, Methodology, Software, Writing – review & editing. **Vasileios Mavromatis:** Funding acquisition, Investigation, Methodology, Validation, Writing – review & editing. **Jacques Schott:** Funding acquisition, Investigation, Resources, Validation, Writing – review & editing.

References

Alvarez C.C., Penkman K., Kröger R., Finch A. A., Clog M., *et al.* (2024). $B(OH)_4^-$ and CO_3^{2-} do not compete for incorporation into aragonite in synthetic precipitations at pH_{total} 8.20 and 8.41 but do compete at pH_{total} 8.59. *Geochim. Cosmochim. Acta* **379**, 39–52.

Anagnostou E., Huang K.-F., You C.-F., Sikes E. L., Sherrell R. M. (2012). Evaluation of boron isotope ratio as a pH proxy in the deep sea coral Desmophyllum dianthus: evidence of physiological pH adjustment. *Earth Planet. Sci. Lett.* **349-350**, 251–260.

Balan E., Noireaux J., Mavromatis V., Saldi G. D., Montoutillout V., Blanchard M., Pietrucci F., Gervais C., Rustad J. R., Schott J. and Gaillardet J. (2018) Theoretical isotopic fractionation between structural boron in carbonates and aqueous boric acid. *Geochim. Cosmochim. Acta* **222**, 117–129.

Balan E., Pietrucci F., Gervais C., Blanchard M., Schott J., and Gaillardet J. (2016). First-principles study of boron speciation in calcite and aragonite. *Geochim. Cosmochim. Acta* **193**, 119–131.

Barkan Y., Paris G., Webb S. M., Adkins J. F. and Halevy I. (2020). Sulfur isotope fractionation between aqueous and carbonate-associated sulfate in abiotic calcite and aragonite. *Geochim. Cosmochim. Acta* **280**, 317–339.

Bethke C. M. (2008). Geochemical and biogeochemical reaction modeling. 2nd Edition. Cambridge University Press. 543 p.

Bots P., Benning L. G., Rickaby R. E. M., and Shaw S. (2011). The role of SO_4 in the switch from calcite to aragonite seas. *Geology* **39**, 331–334.

Branson O. (2018). Boron incorporation into marine CaCO3. In Boron Isotopes: The Fifth Element. Advances in Isotope Geochemistry. H. Marschall and G. Foster editors. Springer International Publishing, pp. 71–105.

Brazier, J.-M., Blanchard, M., Méheut, M., Schmitt, A.D., Schott, J., Mavromatis, V. (2023). Experimental and theoretical investigations of stable Sr isotope fractionation during its incorporation in aragonite. *Geochim. Cosmochim. Acta* **358**, 134–147.

Busenberg E. and Plummer L. N. (1985). Kinetic and thermodynamic factors controlling the distribution of SO_4^{2-} and Na^+ in calcites and selected aragonites. *Geochim. Cosmochim. Acta* **49**, 713–725.

Catanzaro E. J., Champion C. E., Garner E. L., Marinenko G., Sappenfield K. M., Shields W. R. (1970). Boric acid; isotopic and assay standard reference materials. US Natl. Bur. Stan. Spec. Publ. 260 (17), 70 p..

CenCO2PIP Consortium (2023). Toward a Cenozoic history of atmospheric CO_2. *Science* **382**, eadi5177.

Chalk T. B., Standish C. D., D'Angelo C., Castillo K. D., Milton J. A., and Foster G. L. (2021). Mapping coral calcification strategies from in situ boron isotope and trace element measurements of the tropical coral *Siderastrea siderea*. *Sci. Rep.* **11**, 472.

Coenen D., Evans D., Hauzer H., Nambiar R., Jurikova H. et al. (2024). Boron isotope pH calibration of a shallow dwelling benthic nummulitid foraminifera. *Geochim. Cosmochim. Acta* **378**, 217–233.

Comeau S., Tambutté E., Carpenter R. C., Edmunds P. J., Evensen N. R., Allemand D., Ferrier-Pagès C., Tambutté S. and Venn A. A. (2017). Coral calcifying fluid pH is modulated by seawater carbonate chemistry not solely seawater pH. *Proc. Royal Soc. B*: **284**, 20161669.

Davis J. A., Fuller C. C. and Cook A. D. (1987). A model for trace metal sorption processes at the calcite surface: Adsorption of Cd^{2+} and subsequent solid solution formation. *Geochim. Cosmochim. Acta* **51**, 1477–1490 (1987).

DeCarlo T. M., Holcomb M., and McCulloch M. T. (2018). Reviews and syntheses: Revisiting the boron systematics of aragonite and their application to coral calcification. *Biogeosciences* 15, 2819–2834.

Deer W. A., Howie R. A., Zussman, J. (1992). An introduction to the rock-forming minerals. Third edition. The Mineralogical Society of London. 498 p.

Dietzel M., Gussone N. and Eisenhauer A. (2004). Co-precipitation of Sr^{2+} and Ba^{2+} with aragonite by membrane diffusion of CO_2 between 10 and 50 °C. *Chem. Geol.* **203**, 139–151.

Farmer J. R., Branson O., Uchikawa J., Penman D. E., Hönisch B., and Zeebe R. E. (2019). Boric acid and borate incorporation in inorganic calcite inferred from B/Ca, boron isotopes and surface kinetic modeling. *Geochim. Cosmochim. Acta* **244**, 229-247.

Fernández-Díaz L., Fernández-González Á., and Prieto M. (2010). The role of sulfate groups in controlling $CaCO_3$ polymorphism. *Geochim. Cosmochim. Acta* **74**, 6064–6076.

Foster G. L., Pogge von Strandmann P. A. E., and Rae J. W. B. (2010). Boron and magnesium isotopic composition of seawater. *Geochem. Geophys. Geosyst.* **11**(8), Q08015.

Foster G. L. and Rae J. W. B. (2016). Reconstructing ocean pH with boron isotopes in foraminifera. *Annu. Rev. Earth Planet. Sci.* **44**, 207–237.

Franklin M. L. and Morse J. W. (1983). The interaction of manganese(II) with the surface of calcite in dilute solutions and seawater. *Mar. Chem.* **12**, 241–254.

Gabitov R. I., Gaetani G. A., Watson E. B., Cohen A. L. and Ehrlich H. L. (2008). Experimental determination of growth rate effect on U^{6+} and Mg^{2+} partitioning between aragonite and fluid at elevated U^{6+} concentration. *Geochim. Cosmochim. Acta* **72**, 4058–4068.

Goetschl, K.E., Purgstaller, B., Dietzel, M., Mavromatis, V., 2019. Effect of sulfate on magnesium incorporation in low-magnesium calcite. Geochim. Cosmochim. Acta 265, 505–519.

Heberling F. (2025). Surface complexation models for carbonate minerals. *Rev. Mineral. Geochem.* **91B**, *In press: http://dx.doi.org/10.2138/rmg.2025.91B.XX*

Heberling F., Klačić T., Raiteri P., Gale J. D., Eng P. J., Stubbs J. E., Gil-Díaz T., Begović T., and Lützenkirchen J. (2021). Structure and surface complexation at the calcite (104) –water interface. *Environ. Sci. Technol.* **55**, 12403–12413.

Heberling F., Trainor T. P., Lützenkirchen J., Eng P., Denecke M. A., Bosbach D. (2011). Structure and reactivity of the calcite–water interface. *J. Colloid Interface Sci.* **354**, 843–857.

Hemming N. G. and Hanson G. N. (1992). Boron isotopic composition and concentration in modern marine carbonates. *Geochim. Cosmochim. Acta* **56**, 537–543.

Henehan M. J., Rae J. W. B., Foster G. L., Erez J., Prentics K. C. *et al.* (2013). Calibration of the boron isotope proxy in the planktonic foraminifera Globigerinoides ruber for use in palaeo-CO_2 reconstruction. *Earth Planet. Sci. Lett.* **364**, 111–122.

Henehan M. J., Edgar K. M., Foster G. L., Penman D. E., Hull P. M *et al.* (2020). Revisiting the Middle Eocene Climatic Optimum "Carbon Cycle Conundrum" With New Estimates of Atmospheric pCO2 From Boron Isotopes. *Paleoceanogr. Paleoclimatol.* **35**, e2019PA003713.

Henehan M. J., Klei Gebbinck C. D., Wyman J. V. B., Hain M. P., Rae J. W. B. *et al.* (2022). No ion is an island: Multiple ions influence boron incorporation into $CaCO_3$. *Geochim. Cosmochim. Acta* **318**, 510–530.

Hiemstra T.; Van Riemsdijk, W. Bolt G. (1989). Multisite proton adsorption modeling at the solid/solution interface of (hydr) oxides: A new approach: I Model description and evaluation of intrinsic reaction constants. *J. Colloid Interface Sci.* **133**, 91−104.

Holcomb M., Venn A. A., Tambutté E., Tambutté S., Allemand D., Trotter J. and McCulloch M. (2014). Coral calcifying fluid pH dictates response to ocean acidification. *Sci Rep* **4**, 5207.

Holcomb M., DeCarlo T. M., Gaetani G. A., and McCulloch M. (2016). Factors affecting B/Ca ratios in synthetic aragonite. *Chem. Geol.* **437**, 67–76.

Hönisch B., Bijma J., Russell A. D., Spero H. J., Palmer M. R., Zeebe R. E., and Eisenhauer, A. (2003). The influence of symbiont photosynthesis on the boron isotopic composition of foraminifera shells. *Marine Micropaleontology* **49**, 87–96.

Hönisch B., Eggins S. M., Haynes L. L., Allen K. A., Holland K. D., and Lorbacher K. (2019). Boron Proxies in Paleoceanography and Paleoclimatology, Analytical Methods in Earth and Environmental Science Series. John Wiley & Sons, Ltd. 231 p.

Hönisch B., Hemming N. G., Grottoli A. G., Amat A., Hanson G. N. and Bijma J. (2004). Assessing scleractinian corals as recorders for paleo-pH: Empirical calibration and vital effects. *Geochim. Cosmochim. Acta* **68**, 3675–3685.

Johnson C. M., Beard B. L. and Albare`de F. (2004) Overview and general concepts. *Rev. Mineral. Geochem.* **55**, 1–24.

Kaczmarek K., Nehrke G., Misra S., Bijma J. and Elderfield H. (2016). Investigating the effects of growth rate and temperature on the B/Ca ratio and $\delta^{11}B$ during inorganic calcite formation. *Chem. Geol.* **421**, 81–92

Klochko K., Kaufman A. J., Yao W., Byrne R. H. and Tossell, J. A. (2006) Experimental measurement of boron isotope fractionation in seawater. *Earth Planet. Sci. Lett*. **248**, 276-285.

Kontrec, J., Kralj D., Brecevic L., Falini G., Fermani S. et al. (2004). Incorporation of Inorganic Anions in Calcite. *Eur. J. Inorg. Chem.* **2004**, 4579–4585.

Kornicker W. A., Morse J. W. and Damasceno R. N. (1985). The chemistry of Co^{2+} interaction with calcite and aragonite surfaces. *Chem. Geol.* **53**, 229–236.

Krief S., Hendy E. J., Fien M., Yam R., *et al.* (2010). Physiological and isotopic responses of scleractinian corals to ocean acidification. Geochim. Cosmochim. Acta **74**, 4988–5001.

Kwak M. and Shindo, H. (2005). Atomic force microscopic observation of facet formation on various faces of aragonite in aqueous acetic acid. *J. Cryst. Growth* **275**, e1655–e1659.

Langmuir D. (1997). Aqueous Environmental Geochemistry. Prentice-Hall, Inc. 600 p.

Le Goff C., Tambutté E., Venn A. A., Techer N., Allemand D. and Tambutté S. (2017). In vivo pH measurement at the site of calcification in an octocoral. *Sci. Rep.* **7**, 11210.

Leeuw N. H. de and Parker S. C. (1998). Surface structure and morphology of calcium carbonate polymorphs calcite, aragonite, and vaterite: An atomistic approach. *J. Phys. Chem. B* **102**, 2914–2922.

Lemarchand E., Schott J. and Gaillardet, J. (2005) Boron isotopic fractionation related to boron sorption on humic acid and the structure of surface complexes formed. *Geochim. Cosmochim. Acta* **69**, 3519-3533.

Lemarchand E., Schott J. and Gaillardet, J. (2007) How surface complexes impact boron isotope fractionation: Evidence from Fe and Mn oxides sorption experiments. Earth Planet. Sci. Lett. 260, 277-296.

Louvat P., Bouchez J., Paris G., (2010). MC-ICP-MS isotope measurements with direct injection nebulisation (d-DIHEN): optimisation and application to boron in seawater and carbonate samples. *Geostand. Geoanal. Res.* **35**, 75–8.

Mavromatis V., Montouillout V., Noireaux J., Gaillardet J. and Schott J. (2015). Characterization of boron incorporation and speciation in calcite and aragonite from co-precipitation experiments under controlled pH, temperature and precipitation rate. *Geochim Cosmochim. Acta* **150**, 299–313.

Mavromatis V., Brazier J.-M. and Goetschl K. E. (2022). Controls of temperature and mineral growth rate on Mg incorporation in aragonite. *Geochim. Cosmochim. Acta* **317**, 53–64.

Mavromatis V., Brazier J.-M., Goetschl K., Riechelmann S., Dietzel M., and Schott J. (2025). Effect of sulfate on the kinetic and equilibrium magnesium isotope fractionation between low Mg-calcite and fluid. *Geochim. Cosmochim. Acta* **391**, 69–79.

Mavromatis V., Purgstaller B., Louvat P., Faure L., Montouillout V., Gaillardet J., Schott, J. (2021). Boron isotope fractionation during the formation of amorphous calcium carbonates and their transformation to Mg-calcite and aragonite. *Geochim. Cosmochim. Acta* **315**, 152–171.

McCulloch M., Falter J., Trotter J., and Montagna P. (2012). Coral resilience to ocean acidification and global warming through pH up-regulation. *Nat. Clim. Chang.* **2**, 623–627.

Millero F. J., Zhang J., Fiol S., Sotolongo S., Roy R. N., Lee K. and Mane S. (1993). The use of buffers to measure the pH of seawater. *Mar. Chem.* **44**, 143-152.

Mucci A. and Morse J. W. (1983). The incorporation of Mg^{2+} and Sr^{2+} into calcite overgrowths: influences of growth rate and solution composition. *Geochim. Cosmochim. Acta* **47**, 217–233.

Mucci A. and Morse, J. W. (1984). The solubility of calcite in seawater solutions of various magnesium concentration, I_t = 0.697 m at 25 °C and one atmosphere total pressure. *Geochim. Cosmochim. Acta* **48**, 815–822.

Nir O., Vengosh A., Harkness J. S., Dwyer G. S. and Lahav O. (2015). Direct measurement of the boron isotope fractionation factor: reducing the uncertainty in reconstructing ocean paleo-pH. *Earth Planet. Sci. Lett.* **414**, 1–5.

Noireaux J., Mavromatis V., Gaillardet J., Schott J., Montouillout V. *et al.* (2015). Crystallographic control on the boron isotope paleo-pH proxy. *Earth Planet. Sci. Lett.* **430**, 398–407.

Okumura T., Kim H.-J., Kim J.-W., and Kogure T. (2018). Sulfate-containing calcite: crystallographic characterization of natural and synthetic materials. *Eur. J. Miner.* **30**, 929–937.

Parkhurst D. L. and Appelo C. A. J. (2013) Description of input and examples for PHREEQC version 3—A computer program for speciation, batch-reaction, one-dimensional transport, and inverse geochemical calculations. U.S. Geological Survey Techniques and Methods, book 6, chap. A43, 497 p., available only at https://pubs.usgs.gov/tm/06/a43/.

Pingitore N. E., Meitzner G. and Love K. M. (1995). Identification of sulfate in natural carbonates by x-ray absorption spectroscopy. *Geochim. Cosmochim. Acta* **59**, 2477–2483.

Rae J. W. B., Zhang Y. G., Liu X., Foster G. L., Stoll H. M., and Whiteford R. D. M. (2021). Atmospheric CO_2 over the past 66 million years from marine archives. *Annu. Rev. Earth Planet. Sci.* **49**, 1–33 (2021).

Reynaud S., Hemming N. G., Juillet-Leclerc A., and Gattuso J.-P. (2004). Effect of pCO_2 and temperature on the boron isotopic composition of the zooxanthellate coral Acropora sp. *Coral Reefs* **23**, 539–546.

Ring S. J., Henehan M. J., Blukis R. and Blanckenburg F. von. (2025). Adsorption pathways of boron on clay and their implications for boron cycling on land and in the ocean. *Geochim. Cosmochim. Acta* **389**, 74–83.

Rollion-Bard C. and Erez J. (2010). Intra-shell boron isotope ratios in the symbiont-bearing benthic foraminiferan Amphistegina lobifera: Implications for $\delta^{11}B$ vital effects and paleo-pH reconstructions. *Geochim. Cosmochim. Acta* **74**, 1530–1536.

Rollion-Bard C., Blamart D., Trebosc J., Tricot G., Mussi A., and Cuif J.-P. (2011). Boron isotopes as pH proxy: A new look at boron speciation in deep-sea corals using 11B MAS NMR and EELS. *Geochim. Cosmochim. Acta* **75**, 1003–1012.

Sah R. N. and Brown P. H. (1997). Boron determination—a review of analytical methods. *Microchem. J.* **56**, 285–304.

Saldi G. D., Noireaux J., Louvat P., Faure L., Balan E., Schott J. and Gaillardet J. (2018). Boron isotopic fractionation during adsorption by calcite – Implication for the seawater pH-proxy Geochim. Cosmochim. Acta **240**, 255-273.

Sanyal A., Nugent M., Reeder R.J., and Bijma J. (2000). Seawater pH control on the boron isotopic composition of calcite: evidence from inorganic calcite precipitation experiments. *Geochim. Cosmochim. Acta* **64**, 1551–1555.

Sen S., Stebbins J. F., Hemming N. G. and Gosh B. (1994) Coordination environment of B impurities in calcite and aragonite polymorphs: a ^{11}B MAS NMR study. *Am. Mineral*. **79**, 819-825.

Smallwood P. V. (1977). Some aspects of the surface chemistry of calcite and aragonite. Part I: An electrokinetic study.

Smith R. M. and Martell A. E. (1989). Critical stability constants. Volume 6, second supplement. Springer Science & Business Media, LLC. 642 p.

Staudt W. J., Reeder R. J., and Schoonen M. A. A. (1994). Surface structural controls on compositional zoning of SO_4^{2-} and SeO_4^{2-} in synthetic calcite single crystals. *Geochim. Cosmochim. Acta* **58**, 2087–2098.

Sunagawa I., Takahashi Y. and Imai H. (2007). Strontium and aragonite-calcite precipitation. *J. Miner. Pet. Sci.* **102**, 174–181.

Tadier S., Rokidi S., Rey C., Combes C., and Koutsoukos P. G. (2017). Crystal growth of aragonite in the presence of phosphate. *J. Crystal Growth* **458**, 44−52.

Thoenen T., Hummel W., Berner U, and Curti E. (2014). The PSI/Nagra Chemical Thermodynamic Database 12/07. Paul Scherrer Institut:Villigen PSI, Switzerland. Vol. 14-04. 416 p..

Trotter J., Montagna P., McCulloch M., Silenzi S., Reynaud S., Mortimer G., Martin S., Ferrier-Pagès C., Gattuso J.-P. and Rodolfo-Metalpa R. (2011). Quantifying the pH 'vital effect' in the temperate zooxanthellate coral Cladocora caespitosa: Validation of the boron seawater pH proxy. *Earth Planet. Sci. Lett.* **303**, 163–173.

Uchikawa J., Penman D. E., Zachos J. C., and Zeebe R. E. (2015). Experimental evidence for kinetic effects on B/Ca in synthetic calcite: Implications for potential $B(OH)_4^-$ and $B(OH)_3$ incorporation. *Geochim. Cosmochim. Acta* **150**, 171–191.

Uchikawa J., Harper D. T., Penman D. E., Zachos, J. C. and Zeebe, R. E. (2017). Influence of solution chemistry on the boron content in inorganic calcite grown in artificial seawater. *Geochim. Cosmochim. Acta* **218**, 291–307.

Uchikawa J., Penman D. E., Harper D. T., Farmer J. R. *et al.* (2023). Sulfate and phosphate oxyanions alter B/Ca and $\delta^{11}B$ in inorganic calcite at constant pH: Crystallographic controls outweigh normal kinetic effects. *Geochim. Cosmochim. Acta* **343**, 353–370.

Venn A. A., Tambutté E., Holcomb M., Julien L., Allemand D., Tambutté S. (2013). Impact of seawater acidification on pH at the tissue–skeleton interface and calcification in reef corals. *Proc. Natl. Acad. Sci.* **110**, 1634–1639.

Vogl J. and Rosner M. (2011). Production and Certification of a Unique Set of Isotope and Delta Reference Materials for Boron Isotope Determination in Geochemical, Environmental and Industrial Materials. *Geostand. Geoanal. Res.*, **36**(2), 161–175.

Xiao J., Xiao Y. K., Liu C. Q. and Jin Z. D. (2011). Boron isotope fractionation during brucite deposition from artificial seawater. *Clim. Past* **7**, 693–706.

Yin X., Liu F., Liu Q., Zhang Y., Gao C. *et al.* (2023). Boron isotope fractionation between B(OH)3 and B(OH)4 − in aqueous solution: A theoretical investigation beyond the harmonic and Born−Oppenheimer approximations. *Chem. Geol.* **627**, 121455.

Zhang X. Y., Saldi G. D., Schott J., Bouchez J., Kuessner M. Montouillout V., Henehan M., Gaillardet J. (2021). Experimental constraints on Li isotope fractionation during the interaction between detrital material and seawater. *Geochim. Cosmochim. Acta* **292**, 333-347.

Zhong S. and Mucci A. (1989). Calcite and aragonite precipitation from seawater solutions of various salinities: Precipitation rates and overgrowth compositions. *Chem. Geol.* **78**, 283–299.

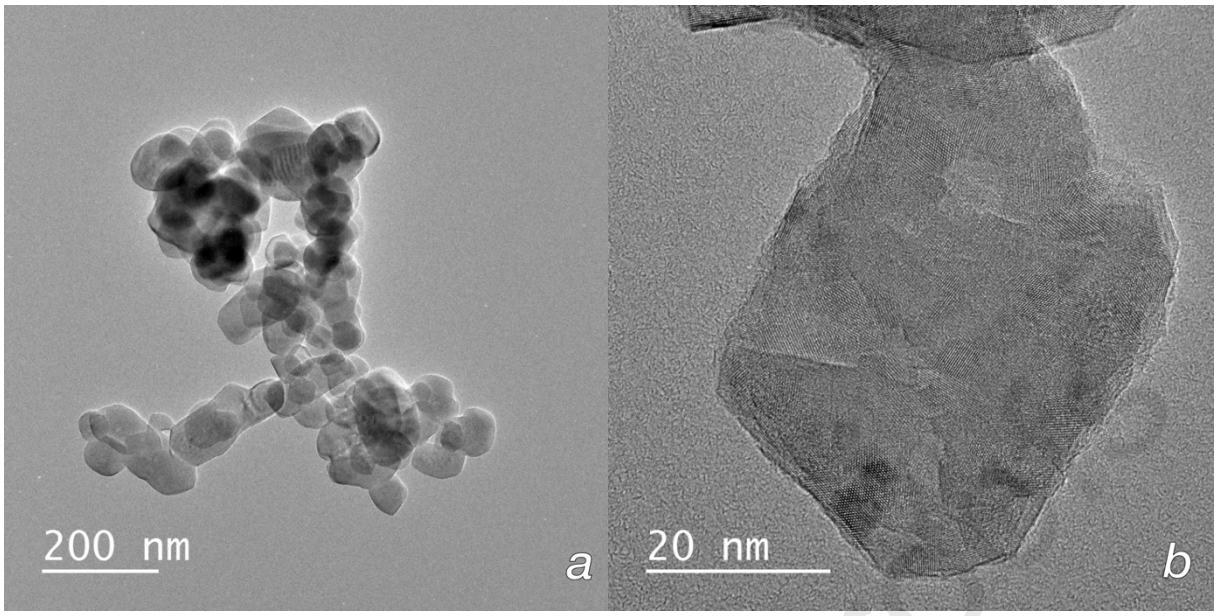

Fig.1. TEM images of the Solvay synthetic nanocalcite used for the boron adsorption experiments in NaCl 0.5 M and artificial seawater (ASW) solutions. EDX analyses and high-resolution imaging confirmed that the single particles consist of pure fully crystalline calcite. Lattice planes and ordered structure are visible inside individual particles under high resolution HAADF-STEM imaging (b).

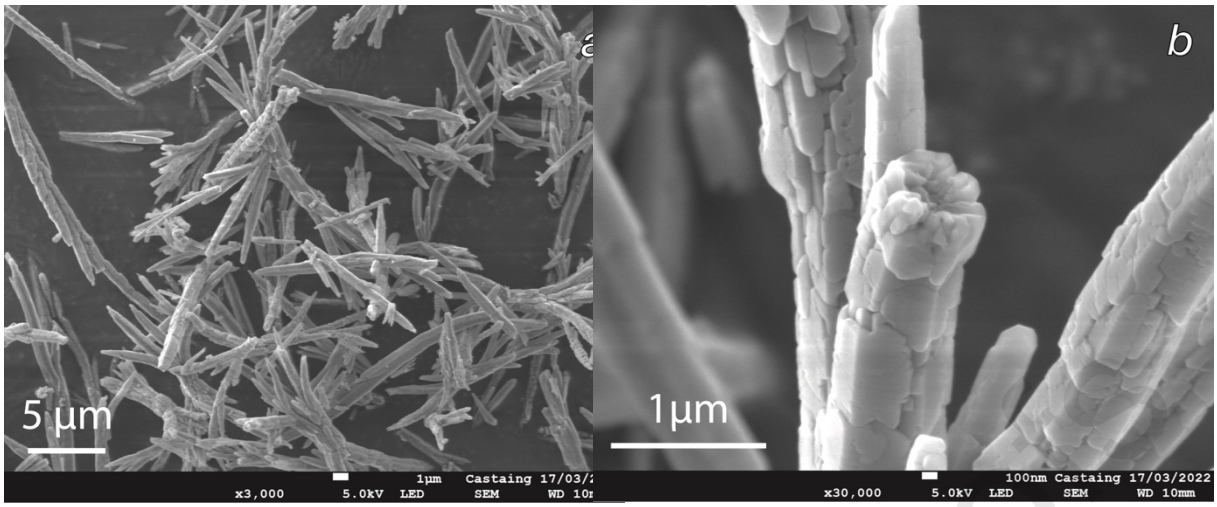

Fig. 2. SEM microphotographs of the synthetic aragonite powder used for boron adsorption experiments in NaCl 0.5 M and artificial seawater (ASW) solutions. The powder consists of aggregates of acicular crystals, which appear to be formed by smaller aragonite microplates, as shown in (b).

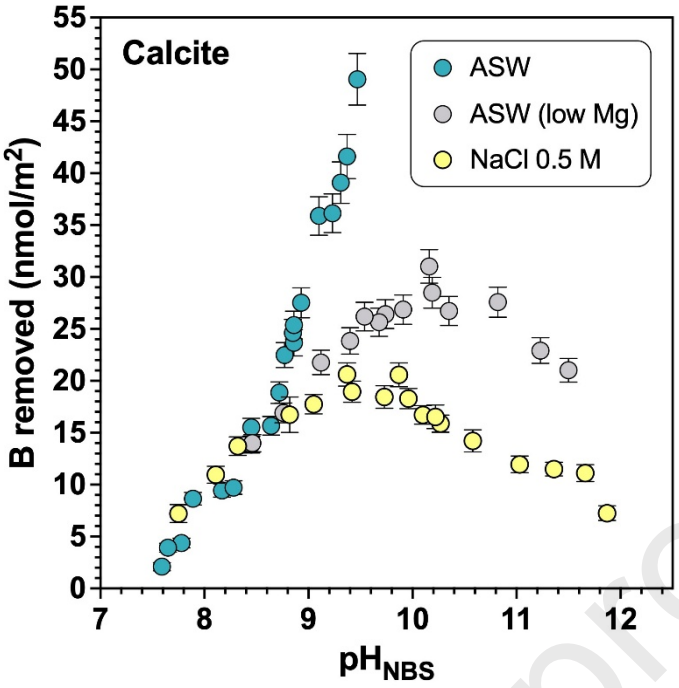

Fig. 3. Surface density of boron removed from the solution in the presence of calcite as function pH in three different aqueous fluids: NaCl 0.5 M; artificial seawater (ASW) and artificial seawater with low Mg concentration (~75 ppm). The illustrated data were obtained for initial B concentrations of ~5 ppm using calcite/water ratios of 278-300 g/L. Data are normalized to the measured BET specific surface area of the starting calcite powder (22.67 m^2/g). Error bars are calculated from the analytical uncertainties of measured B concentrations and SSA_{BET} (± 5%).

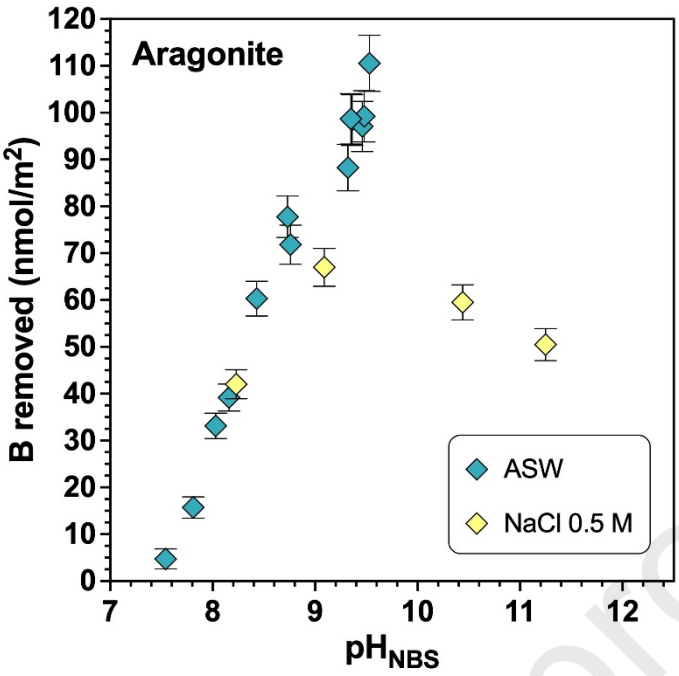

Fig. 4. Surface density of boron removed from the solution in the presence of aragonite as function pH in NaCl 0.5 M and artificial seawater (ASW). All the data were obtained for an initial B concentration of ~5 ppm using a solid/water ratio of 279-300 g/L. Data are normalized to the measured BET specific surface area (4.31 m^2/g) of the aragonite powder. Error bars are calculated from the analytical uncertainties of measured B concentrations and SSA_{BET} (± 5%).

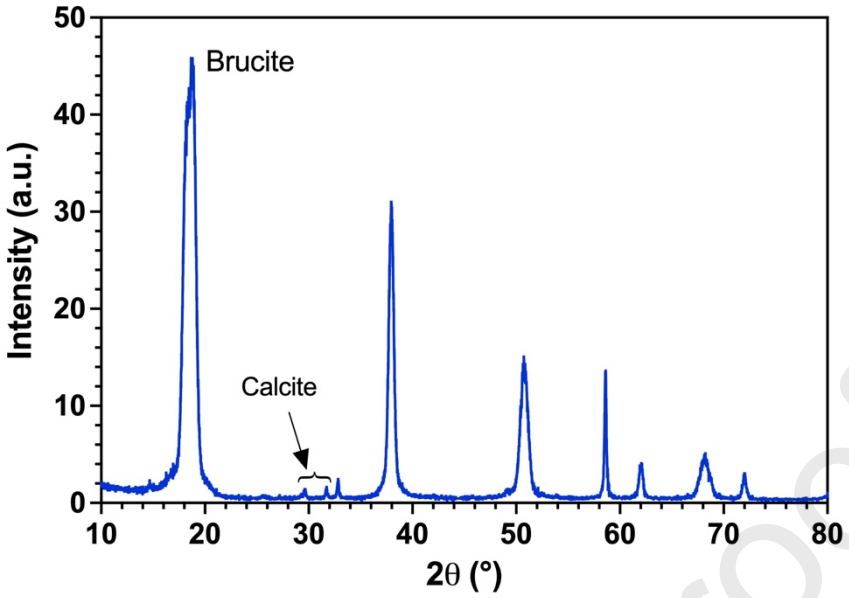

Fig. 5. X-ray diffraction pattern of the solid product formed after the addition of 0.4-1.1 mL of NaOH to artificial seawater. The precipitate consists mainly of brucite with traces of calcite (< 1%).

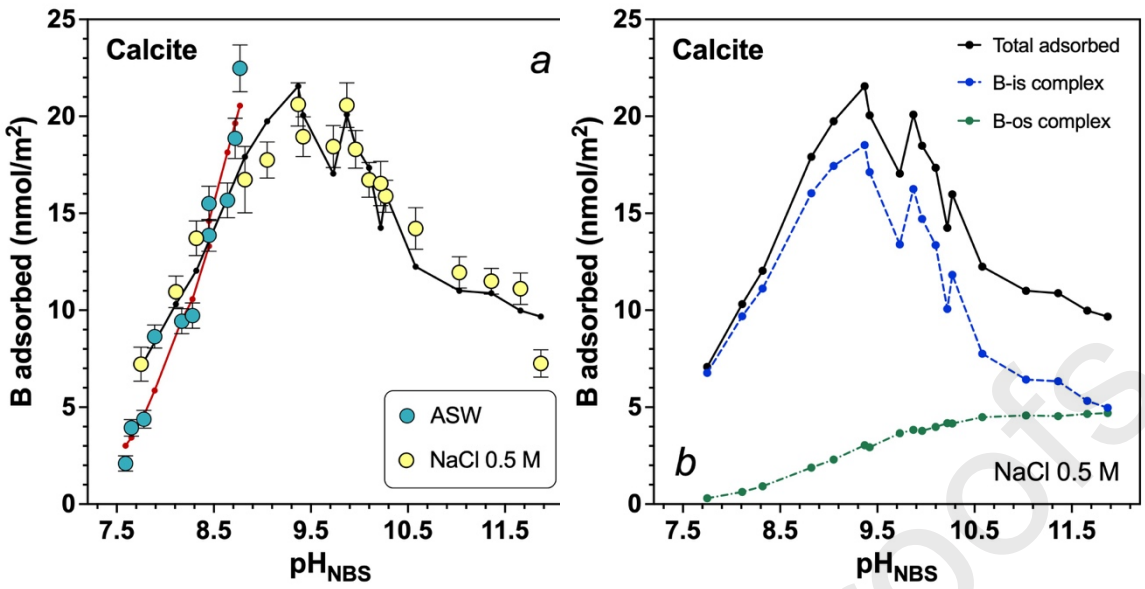

Fig. 6. Results of the fit of the three-plane model (TPM) adopted in this study to measured boron adsorption on calcite in artificial seawater (ASW) (red dots connected by a continuous line) and in NaCl 0.5 M aqueous solutions (black dots connected by a continuous line). The plot in (b) shows the fit to the data in NaCl 0.5M with the relative contribution of the borate inner-sphere complex (B-is) and the borate outer-sphere complex (B-os) as indicated by respectively the dashed blue and the dotted-dashed green lines, respectively, connecting the dots of the same color. Data affected by the saturation of the fluid relative to brucite in seawater were excluded from the fitting procedure and the calculation of B adsorption constants. The scatter observed in the adsorption data at pH 9.4-10 reflects the limited reproducibility (8-12 %) of the experiments in this pH range. (Colors online)

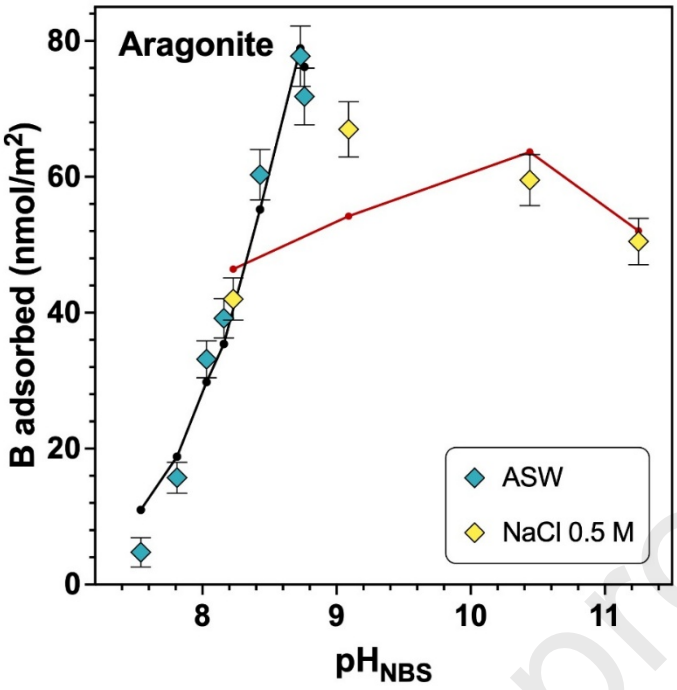

Fig. 7. Results of the fit of the three-plane model (TPM) adapted to the aragonite surface to measured boron adsorption on aragonite in NaCl 0.5 M aqueous solutions (black dots connected by a continuous line) and in artificial seawater (ASW) (red dots connected by a continuous lines). Seawater data affected by the saturation of the fluid relative to brucite were excluded from the fitting procedure and the calculation of B adsorption constants.

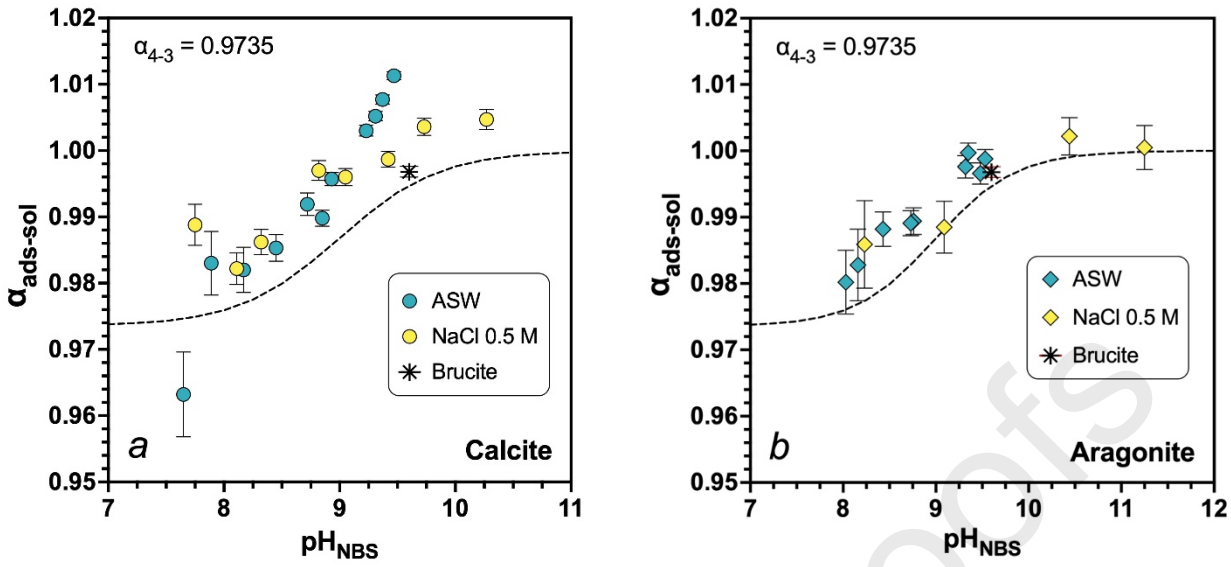

Fig. 8. Boron isotope fractionation factors during adsorption on calcite (a) and aragonite (b) in NaCl 0.5 M (yellow symbols) and artificial seawater (ASW) (turquoise symbols) as a function of pH. Note that ASW data at pH > 9 do not reflect pure boron adsorption (see text). The B isotope fractionation associated with brucite precipitation (black asterisk) is also reported on the two plots. The black dashed line describes the change of the fractionation factor between adsorbed and dissolved borate, calculated for $\alpha_{4\text{-}3}$=0.9735 and assuming no isotope fractionation between the calcite surface and the aqueous solution. (Colors online)

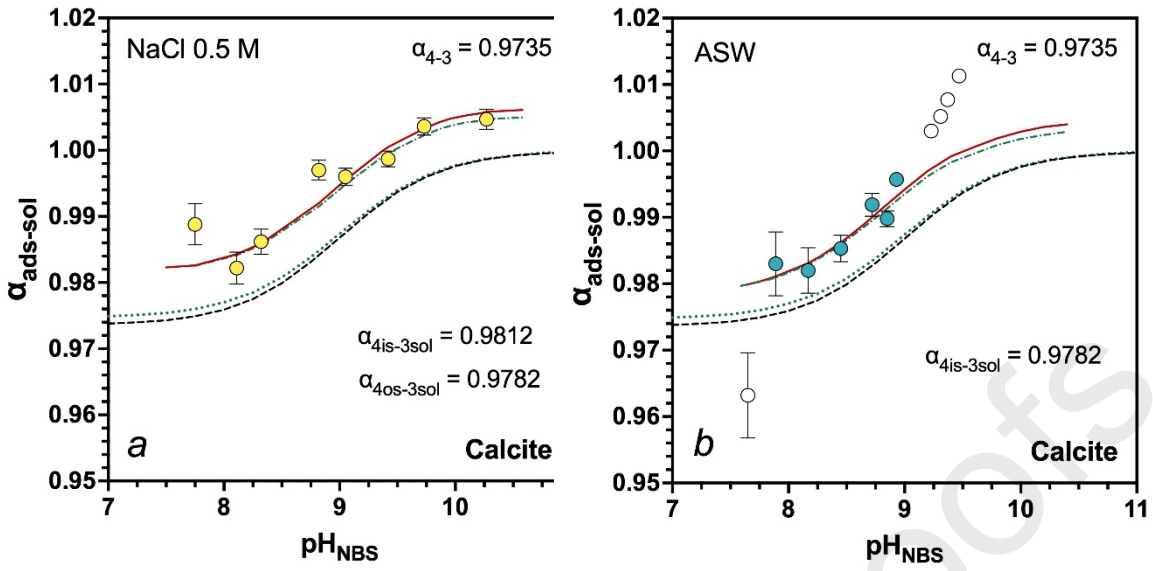

Fig. 9. Model of B isotope fractionation between the calcite surface and the aqueous solution in NaCl 0.5 M solutions (a) and in artificial seawater (b) according to the three-plane model adopted in this work to describe the adsorption of $B(OH)_4^-$ at the calcite/water interface. Continuous red lines represent the least-square fit of Eq. (16) to the experimental data reported on the plots (yellow and turquoise circles). The black dashed line describes the change with pH of the fractionation factor between adsorbed and dissolved borate, calculated for $\alpha_{4\text{-}3}$=0.9735 and assuming no isotope fractionation between adsorbed and dissolved borate species. According to the fitted values of $\alpha_{4ex-3sol}$ and $\alpha_{4ads-3sol}$ adsorbed borate is 4.7-7.7 ‰ heavier than the aqueous ion. Note that the model in (b) did not take into account the empty circles, which correspond to the outlier at pH = 7.65 and the data affected by brucite precipitation (pH > 9). The two plots also report the results (dotted and dotted-dashed green lines) obtained using a fractionation factor between $B(OH)_3$ and $B(OH)_4^-$ of 26 ‰ (α_{4-3}= 0.9747), as proposed by Nir et al. (2015). (Colors online)

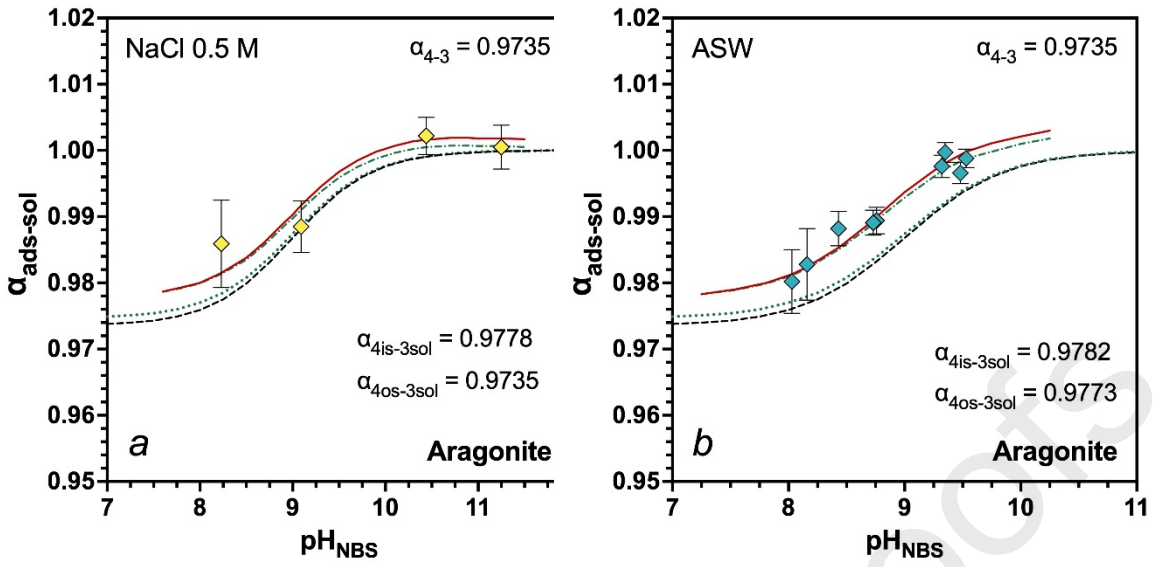

Fig. 10. Model of B isotope fractionation between the aragonite surface and the aqueous solution in NaCl 0.5 M solutions (a) and in artificial seawater (b) according to the three-plane model (TPM) used to describe the adsorption of $B(OH)_4^-$ at the aragonite/water interface. Continuous red lines represent the least-square fit of Eq. (16) to the experimental data reported on the plots (yellow and turquoise diamonds). The black dashed line describes the change with pH of the fractionation factor between adsorbed and dissolved borate, calculated for $\alpha_{4\text{-}3}$= 0.9735 and assuming no isotope fractionation between adsorbed and dissolved borate species. According to the fitted values of $\alpha_{4ex-3sol}$ and $\alpha_{4ads-3sol}$ adsorbed borate is 3.8-4.7 ‰ heavier than the aqueous ion. The two plots also report the results (dotted and dotted-dashed green lines) obtained using a fractionation factor between $B(OH)_3$ and $B(OH)_4^-$ of 26 ‰ (α_{4-3}= 0.9747), as proposed by Nir et al. (2015). (Colors online)

Table 1. Composition of the artificial seawater solutions used for the experiments of boron adsorption on calcite and aragonite (n.a = not analyzed).

Sea water type	Na ppm	Ca ppm	K ppm	Mg ppm	Sr ppm	SO_4^{2-} ppm	Cl$^-$ ppm	Alkalinity eq/l
standard ASW	10962.6	419.1	360.5	1307.1	7.8	2629.3	n.a	n.a
low-Mg ASW	10910.2	397.2	364.3	123.7	7.9	n.a	n.a	n.a

Table 2. Summary of the calcite surface complexation reactions and corresponding stability constants defined by the Three Plane Model (TPM) developed by Heberling et al. (2011, 2021). The inner and outer layer capacitance values assumed for each model were, respectively, C_1= 0.2 F/m^2 and C_2=1.5 F/m^2. The surface density of both >Ca and >CO_3 sites was assumed to be equal to 4.95 nm^{-2}.

Calcite/aragonite surface reactions	log K^0_{int} (25 °C, I=0)
Inner-sphere (de-)protonation reactions	
1. $> CO_3^{-0.5} + H^+ => CO_3H^{+0.5}$	1.3 ±0.1
2. $> CaOH^{-0.5} + H^+ => CaOH_2^{+0.5}$	13.38 ±0.04
Outer-sphere ion-binding reactions	
(">…" equally defines $> Ca$ *and* $> CO_3$ *species*	
3. $> \ldots OH^{-0.5} + Na^+ => \ldots OHNa^{+0.5}$	0.5 ±0.1
4. $> \ldots OH^{-0.5} + Ca^{2+} => \ldots OHCa^{+1.5}$	-0.69 ±0.02
5. $> \ldots OH_2^{+0.5} + Cl^- => \ldots OH_2Cl^{-0.5}$	0.61 ±0.08
6. $> \ldots OH_2^{+0.5} + HCO_3^- => \ldots OH_2HCO_3^{-0.5}$	0.37 ±0.05
7. $> \ldots OH_2^{+0.5} + CO_3^{2-} => \ldots OH_2CO_3^{-1.5}$	1.91 ±0.38

Table 3. Summary of the boron adsorption experiments carried out on calcite in NaCl 0.5 M solutions. All runs were conducted using synthetic Solvay calcite with a specific surface area of 22.67 m^2/g. Note that the experiments were conducted at equilibrium conditions. The reported values of TDIC and log pCO_2 were calculated assuming thermodynamic equilibrium between the aqueous fluid and calcite. Refer to Table S1 in the Supplementary Material for the starting conditions of each experiment.

Run #	pH	Δ[B] ppm	$\%B_{ads}$	B_{ads} nmol/m^2	[Ca] ppm	TDIC mM	log pCO_2
BW-40	7.75	-0.495	8.8	7.2	138.19	2.24	-2.82
BW-41	8.11	-0.751	13.3	11.0	97.06	1.40	-3.39
BW-42	8.32	-0.940	16.7	13.7	76.63	1.12	-3.70
BW-43	8.82	-1.144	20.4	16.7	55.39	0.57	-4.56
BW-46	9.05	-1.215	22.3	17.7	49.96	0.42	-4.98
BW-44	9.37	-1.413	25.1	20.6	40.89	0.33	-5.53
BW-58	9.42	-1.302	24.8	19.0	39.03	0.32	-5.61
BW-52	9.73	-1.271	23.6	18.4	24.25	0.39	-6.02
BW-45	9.87	-1.409	25.1	20.6	28.69	0.30	-6.37
BW-47	9.96	-1.249	23.3	18.3	26.11	0.31	-6.51
BW-48	10.1	-1.147	21.3	16.7	22.38	0.34	-6.72

Run #	pH	Δ[B] ppm	$\%B_{a_{ds}}$	B_{ads} nmol/m^2	[Ca] ppm	TDIC mM	log pCO_2
BW-53	10.22	-1.131	21.3	16.5	15.61	0.47	-6.81
BW-49	10.27	-1.088	20.2	15.9	18.76	0.38	-6.99
BW-54	10.58	-0.974	18.2	14.2	10.92	0.62	-7.37
BW-55	11.03	-0.817	15.4	12.0	8.79	0.75	-8.17
BW-59	11.36	-0.788	15.0	11.5	8.81	0.75	-8.83
BW-56	11.66	-0.761	14.3	11.1	7.30	0.92	-9.34
BW-57	11.87	-0.497	9.3	7.3	6.88	1.00	-9.72

Table 4. Summary of the boron adsorption experiments carried out on calcite in artificial seawater (ASW). All runs were conducted using synthetic Solvay calcite with a specific surface area of 22.67 m^2/g. The last two columns report the saturation indexes of the aqueous solutions with respect to gypsum and brucite (SI_{Gp} and SI_{Brc}). SI_{Gp} for the experiments in which SO_4^{2-} was not analyzed were estimated assuming SO_4^{2-} concentrations measured for similar pH values. Note that the experiments were conducted at equilibrium conditions. The reported values of TDIC and log pCO_2 were calculated assuming thermodynamic equilibrium between the aqueous fluid and calcite. Refer to Table S1 in the Supplementary Material for the starting conditions of each experiment.

un #	H_{NBS}	[B]	B_{ads}	ads	]	[Na]	[Ca]	[K]	[Mg]	[Sr]	[SO_4^{-2}]	DIC	og pCO_2	I_{Gp}	I_{Brc}
		pm		mol/m^2	r	pm	pm	pm	ppm	pm	pm	M			
W-17	.59	0.165	.2	.1	2	220.2	46.4	.5	47.2	4.1	.a.	.402	2.90	0.69	3.55
W-16	.65	0.310	.0	.9	3	275.6	54.1	0.4	53.0	4.8	589.1	.246	3.01	0.69	3.43
W-11	.78	0.322	.9	.4	2	175.8	53.8	5.6	18.3	4.7	.a.	.955	3.25	0.59	3.17
W-10	.89	0.634	1.6	.6	8	323.0	70.4	1.5	37.9	4.8	588.0	.757	3.47	0.71	2.94
W-09	.17	0.647	1.8	.4	9	370.9	74.2	3.7	56.8	4.7	368.2	.423	4.02	0.67	2.40
W-19	.28	0.666	2.9	.7	9	481.5	76.2	.6	28.3	4.2	.a.	.343	4.23	0.69	2.17
W-05	.45	0.950	8.5	3.9	1	212.8	88.4	.9	63.8	4.5	.a.	.255	4.55	0.63	1.85

W-06	.45	1.062	9.2	5.5	1 261.0	80.4	.4	69.3	4.8	441.0	.244	4.57	0.69	1.84
W-07	.64	1.074	9.5	5.7	1 562.9	91.2	.2	78.5	4.8	.a.	.178	4.93	0.70	1.46
W-22	.67	2.057	9.5	0.0	3 231.9	106.9	.2	217.6	5.0	.a.	.176	4.96	0.72	1.47
W-08	.72	1.290	3.4	8.9	1 281.6	79.6	.0	71.5	4.7	403.6	.150	5.11	0.69	1.30
W-12	.77	1.536	8.0	2.5	2 237.5	87.2	.3	105.9	4.8	.a.	.140	5.20	0.71	1.21
W-14*	.85	1.686	0.7	4.6	2 360.1	101.0	1.1	125.5	4.0	512.2	.129	5.34	0.73	1.06
W-13*	.86	1.624	9.6	3.7	2 272.3	90.9	.8	121.9	4.1	.a.	.123	5.37	0.72	1.04
W-15*	.86	1.742	1.7	5.4	2 204.5	99.5	.1	157.7	4.1	.a.	.126	5.36	0.73	1.05
W-18*	.93	1.886	6.8	7.5	2 309.1	92.5	1.0	145.7	4.9	427.8	.112	5.51	0.71	0.91
W-50*	.09	2.630	7.0	8.5	3 .a.	.a.	.a.	.a.	.a.	.a.	.090	5.83	0.72	0.59
W-23*	.10	2.462	7.7	5.9	3 153.6	97.7	7.0	261.9	4.2	.a.	.089	5.84	0.72	0.62

W-24*	.23	2.476	8.0	6.1	207.2	98.6	0.5	313.1	4.1	437.2	.077	6.09	0.71	0.39
W-25*	.31	2.677	1.7	9.1	196.8	102.6	17.1	377.0	4.1	415.9	.071	6.24	0.71	0.27
W-20*	.36	2.409	6.9	5.2	362.8	99.5	1.4	273.7	4.0	.a.	.068	6.35	0.70	0.12
W-28*	.37	2.841	4.7	1.6	346.8	98.9	21.1	436.5	4.0	441.6	.066	6.36	0.71	0.20
W-34*	.47	3.363	0.5	9.1	.a.	130.8	9.9	579.3	4.3	359.5	.065	6.49	0.74	0.10

*Samples not reflecting pure adsorption

Table 5. Summary of the boron adsorption experiments carried out on calcite in artificial seawater (ASW) with initially low Mg content (~75 ppm). All runs were conducted using synthetic Solvay calcite with a specific surface area of 22.67 m^2/g. The last two columns report the saturation indexes of the aqueous solutions with respect to gypsum and brucite (SI_{Gp} and SI_{Brc}). n.a. = not analyzed; n.d. = not determined. Note that SI_{Gp} was calculated using the SO_4^{2-} concentration of the initial seawater solution. Note that the experiments were conducted at equilibrium conditions. The reported values of TDIC and log pCO_2 were calculated assuming thermodynamic equilibrium between the aqueous fluid and calcite. Refer to Table S1 in the Supplementary Material for the starting conditions of each experiment.

un #	H_{NBS}	[B]	B_{ads}	ads	] [Na]	[Ca]	[K]	[Mg]	[Sr]	[SO $_4^{-2}$]	DIC	og pCO_2	I_{Gp}	I_{Brc}
		pm		mol/ m^2	ı pm	pm	pm	ppm	pm	pm	M			
W-39	.46	0.959	7.3	3.99	1 .a.	274.9	.9	1.4	5.7	.a.	.557	4.14	0.97	2.78
W-38	.76	1.160	1.0	6.91	1 .a.	282.3	5.4	6.2	5.8	.a.	.326	4.72	1.00	2.20
W-37	.12	1.493	7.1	1.77	2 .a.	278.1	.6	2.7	5.8	.a.	.173	5.45	0.98	1.49
W-36	.40	1.634	9.6	3.84	2 .a.	283.1	0.8	0.5	5.8	.a.	.125	5.99	1.00	0.97
W-35	.54	1.794	2.4	6.19	2 .a.	285.8	.6	9.1	5.8	.a.	.114	6.25	1.02	0.77
W-29	.68	1.757	4.1	5.64	2 293.2	291.1	15.8	.0	5.9	.a.	.095	6.55	0.99	0.60
W-26	.74	1.811	4.9	6.43	2 139.9	308.4	6.3	13.9	6.0	.a.	.105	6.60	1.06	0.61

W-30	.91	1.841	5.7	6.86	303.1	307.7	7.2	30.6	6.0	.a.	.093	6.94	1.06	0.41
W-51*	0.16	2.116	8.1	1.01	.a.	.a.	.a.	.a.	.a.	.a.	.a.	.d.	.d.	.d.
W-31*	0.19	1.953	7.6	8.49	346.0	309.5	12.0	39.6	6.0	.a.	.084	7.49	1.07	.06
W-27*	0.35	1.832	5.4	6.73	68.8	310.9	6.0	51.4	5.6	.a.	.082	7.80	1.08	.20
W-32*	0.82	1.884	6.6	7.58	268.6	303.9	11.2	63.3	5.2	.a.	.072	8.77	1.05	.83
W-21*	1.23	1.566	0.6	2.92	316.6	305.7	14.7	72.1	3.8	.a.	.072	9.57	1.06	.10
W-33*	1.50	1.441	7.8	1.03	268.2	259.4	26.9	75.3	1.3	.a.	.052	10.26	0.91	.92

*Samples not reflecting pure adsorption

Table 6. Summary of the boron adsorption experiments carried out on aragonite in NaCl 0.5 M aqueous solutions. All runs were conducted using synthetic aragonite powder with a specific surface area of 4.31 m^2/g. All the experiments were conducted at equilibrium conditions. The reported values of TDIC and log pCO_2 were calculated assuming thermodynamic equilibrium between the aqueous fluid and aragonite. Refer to Table S2 in the Supplementary Information for the starting conditions of each experiment.

Run #	pH_{NBS}	Δ[B] ppm	$\%B_{ads}$	B_{ads} nmol/m^2	[Ca] ppm	TDIC mM	log pCO_2
BS-20	8.23	-0.547	10.4	42.02	77.48	1.714	-3.40
BS-21	9.09	-0.871	16.2	66.99	19.00	1.050	-4.61
BS-22	10.44	-0.776	14.5	59.51	11.15	0.641	-7.07
BS-23	11.25	-0.656	12.3	50.48	6.90	1.054	-8.44

Table 7. Summary of the boron adsorption experiments carried out on aragonite in artificial seawater (ASW). All runs were conducted using synthetic aragonite powder with a specific surface area of 4.31 m^2/g. The last two columns report the saturation indexes of the aqueous solutions with respect to gypsum and brucite (SI_{Gp} and SI_{Brc}). n.a. = not analyzed. Note that, where SO_4^{2-} concentrations are missing, SI_{Gp} was calculated either using the SO_4^{2-} concentration of the initial seawater solution or the value of the closest pH for which sulfate concentration was measured. All the experiments were conducted at equilibrium conditions. The reported values of TDIC and log pCO_2 were calculated assuming thermodynamic equilibrium between the aqueous fluid and aragonite. Refer to Table S2 in the Supplementary Information for the starting conditions of each experiment.

Run #	pH_{NBS}	Δ[B] ppm	B_{ads} %	B_{ads} nmol/m^2	Δ[Na] ppm	Δ[Ca] ppm	Δ[K] ppm	Δ[Mg] ppm	Δ[Sr] ppm	Δ[SO_4^{-2}] ppm	TDIC (calc) mM	log pCO_2	SI_{Gp}	SI_{Brc}
BS-08	7.54	-0.066	1.3	4.74	-103.5	4.3	-10.7	4.7	-1.1	-150.2	1.813	-2.74	-0.53	-3.64
BS-07	7.81	-0.219	4.2	15.72	-100.9	-22.0	-15.6	-1.8	-1.6	-187.9	1.136	-3.21	-0.59	-3.10
BS-15	8.03	-0.461	8.5	33.15	-93.8	-19.9	-45.6	-1.6	-87.3	0.894	-3.54	-0.67	-2.69
BS-11	8.16	-0.547	10.6	39.18	-134.3	-42.5	-12.6	8.7	-1.5	-37.6	0.563	-3.88	-0.59	-2.40
BS-19	8.43	-0.839	15.5	60.31						-121.2	0.320	-4.43	-0.59	-1.86
BS-16	8.73	-1.083	20.0	77.77		-134.7	-28.7	-48.5	-2.0	-91.6	0.261	-4.88	-0.60	-1.29

B S-12	8. 76	- 1.002	19 .7	71.8 2	- 118.0	- 63.5	- 25.5	5 .3	- 1.8	- 154.6	0. 191	- 5.06	- 0.61	- 1.20
B S-13*	9. 32	- 1.149	22 .5	88.2 7	- 42.0	- 70.0	- 21.8	- 9.1	- 2.3	- 87.6	0. 096	- 6.17	- 0.73	- 0.09
B S-18*	9. 35	- 1.374	25 .3	98.6 6	-	-	-	-	-	- 87.9	0. 093	- 6.23	- 0.63	- 0.04
B S-10*	9. 36	- 1.277	24 .8	98.4 3	- 124.7	- 70.9	- 22.7	- 28.9	- 2.1		0. 093	- 6.25	- 0.63	- 0.02
B S-14*	9. 46	- 1.261	24 .8	97.0 6	- 71.6	- 42.5	- 18.0	- 37.7	- 2.6		0. 079	- 6.49	- 0.63	0 .18
B S-17*	9. 48	- 1.289	24 .0	99.2 3	-	- 147.9	- 21.5	- 79.2	- 2.5	- 71.0	0. 110	- 6.35	- 0.62	0 .19
B S-09*	9. 53	- 1.438	27 .9	110. 56	- 112.4	- 69.6	- 20.1	- 10.4	- 2.0	- 36.0	0. 081	- 6.59	- 0.59	0 .33

*Samples not reflecting pure adsorption

Table 8. Summary of the $CaCO_3$-free suspension in which boron was adsorbed or coprecipitated with a secondary phase (brucite) following addition of the listed amounts of NaOH 1M to artificial seawater. In the BM experiments boron was added to the suspension after NaOH and a period of 48 hours. In the BQ experiments boron was added to the seawater solution before NaOH. The Table reports the saturation indexes of the aqueous solutions with respect to gypsum and brucite (SI_{Gp} and SI_{Brc}) and the logarithm of CO_2 partial pressure assuming equilibrium of each experimental solution with respect to calcite. Note that SI_{Gp} was calculated using the initial aqueous concentration of SO_4^{2-}. The uncertainty on SI_{Brc} is related to the different assumptions made in doing the calculations (see text). The last column list the values of the boron partition coefficient (K_d) between brucite and the aqueous solution.

Run #	pH_{NBS}	NaOH 1 M	Δ[B] ppm	$\%B_{rem}$	Δ[Ca] ppm	Δ[K] ppm	Δ[Mg] ppm	Δ[Sr] ppm	SI_{Gp}	SI_{Brc}	log pCO_2	K_d
BM-01	9.44	0.209	-0.312	6.3	-56.9	-17.4	-149.0	0.2	-0.6	0.0±0.1	-6.5	189
BM-02	9.45	0.314	-0.412	8.4	-57.9	-18.8	-176.2	0.1	-0.6	0.0±0.1	-6.6	217
BM-03	9.48	0.629	-0.964	19.6	-64.0	-36.4	-344.6	0.1	-0.6	0.0±0.1	-6.6	295
BM-04	9.56	1.154	-1.420	28.9	-57.8	-34.5	-600.5	-0.1	-0.6	0.0±0.1	-6.8	282
BQ-05	9.49	0.210	-0.877	16.0	-11.6	-17.3	-87.8	0.0	-0.6	0.0±0.2	-6.7	908
BQ-06	9.53	0.314	-1.219	22.3	-28.7	-25.0	-162.6	0.1	-0.6	0.0±0.3	-6.8	737

Run #		pH_{NBS}	NaOH 1 M	Δ[B] ppm	B_{rem} %	Δ[Ca] ppm	Δ[K] ppm	Δ[Mg] ppm	Δ[Sr] ppm	SI_{Gp}	SI_{Brc}	log pCO_2	K_d
-07	BQ	9.54	0.629	-1.948	35.8	-39.3	-34.5	-316.7	0.1	0.6	0.0 ±0.2	-6.8	734
-08	BQ	9.60	1.158	-2.706	49.8	-57.6	-36.2	-593.8	0.3	0.6	0.0 ±0.2	-6.9	697

Table 9. Summary of the $B(OH)_4^-$ adsorption constants determined for calcite and aragonite (reactions 3-4) in NaCl solutions and artificial seawater and corresponding isotope fractionation factor for each adsorbed species relative to dissolved trigonal boron.

Mineral	Medium	log K_{B-is}^{int} (25 °C. *I=0*)	log K_{B-os}^{int} (25 °C. *I=0*)	χ^2	$\alpha_{4is-3sol}$	$\alpha_{4os-3sol}$
Calcite	NaCl 0.5 M	-7.15 ±0.01	+0.55 ±0.01	2.16	0.9812 ±0.001	0.9782 ±0.002
	ASW	-7.83 ±0.01	-0.86 ±0.01	4.30	0.9782 ±0.002	n.d.
	NaCl 0.01 M*	-7.51 ±0.01*	+0.72 ±0.01*	0.95	0.9763 ±0.001	0.9787 ±0.001
Aragonite	NaCl 0.5 M	-6.40 ±0.01	+1.44 ±0.01	4.64	0.9778 ±0.003	0.9735 ±0.001
	ASW	-7.55 ±0.01	+2.30 ±0.01	2.84	0.9782 ±0.003.	0.9773 ±0.003

*Data from Saldi et al. (2018)

Table 10. Boron isotopic data isotopic data for the adsorption experiments conducted with calcite in NaCl 0.5 M and artificial seawater (ASW) solutions.

	Run #	pH	$X_{B\text{-}ads}$	$\delta^{11}B_{sol} \pm 2\sigma$ ‰	$\delta^{11}B_{ads} \pm 2\sigma$ ‰	$\Delta^{11}B_{a\,ds-sol} \pm 2\sigma$ ‰	$\alpha_{ad\,s-sol} \pm 2\sigma$
ASW	B-W-16	7.65	0.06	2.23 ± 0.29	-35.26 ±6.61	-37.49 ±6.61	0.9632 ±0.0064
	B-W-10	7.89	0.12	1.97 ± 0.55	-15.19 ±4.82	-17.16 ±4.85	0.9830 0.0048
	B-W-09	8.17	0.12	2.13 ± 0.35	-16.03 ±3.46	-18.16 ±3.48	0.9820 ±0.0034
	B-W-06	8.45	0.19	2.81 ± 0.35	-11.98 ±2.04	-14.80 ±2.07	0.9853 ±0.0020
	B-W-08	8.72	0.23	1.88 ± 0.37	-6.23 ±1.66	-8.10 ±1.70	0.9919 ±0.0017
	B-W-14	8.85	0.31	3.13 ± 0.35	-7.15 ±1.18	-10.28 ±1.23	0.9898 ±0.0012
	B-W-18	8.93	0.37	1.56 ± 0.35	-2.73 ±0.94	-4.29 ±1.01	0.9957 ±0.0010
	B-W-24	9.23	0.48	-1.48 ± 0.35	1.56 ±0.68	3.04 ±0.76	1.0030 ±0.0008
	B-W-25	9.31	0.52	-2.71 ± 0.35	2.49 ±0.61	5.20 ±0.71	1.0052 ±0.0007
	B-W-28	9.37	0.55	-4.19 ± 0.35	3.44 ±0.57	7.63 ±0.67	1.0077 ±0.0007
	B-W-34	9.47	0.61	-6.85 ± 0.35	4.43 ±0.50	11.28 ±0.61	1.0113 ±0.0006
NaCl	B-W-40	7.75	0.09	0.91 ±0.28	-10.38 ±3.10	-11.28 ±3.11	0.9888 ±0.0031

0.5 M	**B W-41**	8.1 1	0. 13	2.29 ±0.35	- 15.63±2.40	-17.93 ±2.43	0.98 22 ±0.0024
	B W-42	8.3 2	0. 17	2.23 ±0.35	- 11.69 ±1.85	-13.92 ±1.88	0.98 62 ±0.0019
	B W-43	8.8 2	0. 20	0.53 ±0.35	-2.49 ±1.45	-3.02 ±1.49	0.99 70 ±0.0015
	B W-46	9.0 5	0. 22	0.80 ±0.35	-3.19 ±1.30	-3.99 ±1.34	0.99 60 ±0.0013
	B W-58	9.4 2	0. 25	0.23 ±0.35	-1.07 ±1.13	-1.30 ±1.19	0.99 87 ±0.0012
	B W-52	9.7 3	0. 24	-0.95 ±0.35	2.69 ±1.20	3.64 ±1.25	1.00 36 ±0.0013
	B W-49	10. 27	0. 20	-1.04 ±0.35	3.66 ±1.46	4.69 ±1.51	1.00 47 ±0.0015

Table 11. Boron isotopic data for the adsorption experiments conducted with aragonite in NaCl 0.5 M and artificial seawater (ASW) and those associated with the precipitation of brucite from ASW in the absence of $CaCO_3$ powders (run BQ-08).

	Run #	pH	$X_{B\text{-}ads}$	$\delta^{11}B_{sol} \pm 2\sigma$ ‰	$\delta^{11}B_{ads} \pm 2\sigma$ ‰	$\Delta^{11}B_{a\ ds-sol} \pm 2\sigma$ ‰	$\alpha_{ad\ s-sol} \pm 2\sigma$
ASW	BS-07	7.81	0.04	1.97 ±1.09	-45.15 ±28.28	-47.11 ±28.30	0.9540 ±0.0270
	BS-15	8.03	0.09	1.68 ±0.35	-18.28 ±4.92	-19.96 ±4.93	0.9802 ±0.0048
	BS-11	8.16	0.11	1.81 ±0.57	-15.49 ±5.47	-17.31 ±5.50	0.9828 ±0.0054
	BS-19	8.43	0.16	1.82 ±0.35	-10.06 ±2.58	-11.89 ±2.60	0.9882 ±0.0026
	BS-16	8.73	0.20	2.16 ±0.35	-8.75 ±1.94	-10.92 ±1.97	0.9891 ±0.0019
	BS-12	8.76	0.20	2.08 ±0.35	-8.62 ±1.98	-10.70 ±2.01	0.9894 ±0.0020
	BS-13	9.32	0.23	0.53 ±0.35	-1.92 ±1.69	-2.45 ±1.73	0.9976 ±0.0017
	BS-18	9.35	0.25	0.06 ±0.35	-0.26 ±1.48	-0.32 ±1.52	0.9997 ±0.0015
	BS-17	9.48	0.24	0.79 ±0.35	-2.58 ±1.58	-3.36 ±1.62	0.9966 ±0.0016
	BS-09	9.53	0.28	0.30 ±0.35	-0.86 ±1.32	-1.16 ±1.37	0.9988 ±0.0014
NaCl	BS-20	8.23	0.10	1.39 ±0.72	-12.81 ±6.69	-14.20 ±6.73	0.9859 ±0.0066

0.5 M	BS-21	9.09	0.16	1.78 ±0.68	-9.74 ±3.87	-11.52 ±3.93	0.9885 ±0.0039
	BS-22	10.44	0.14	-0.41 ±0.35	1.80 ±2.78	2.21 ±2.80	1.0022 ±0.0028
	BS-23	11.25	0.12	-0.15 ±0.35	-45.15 ±28.28	0.51 ±3.33	1.0005 ±0.0033
AS W	BQ-08	9.60	0.50	1.60 ±0.38	-1.65 ±0.66	-3.24 ±0.76	0.9968 ±0.0008